J. Fluid Mech. (2008), *vol.* 617, *pp.* 51–86.
doi:10.1017/S0022112008003789 Printed in the United Kingdom

Mixing by random stirring in confined mixtures

J. DUPLAT[1] AND E. VILLERMAUX[2]†

[1]Aix-Marseille Université, IUSTI, 13453 Marseille Cedex 13, France

[2]Aix-Marseille Université, IRPHE, 13384 Marseille Cedex 13, France

(Received 7 May 2007 and in revised form 29 July 2008)

We study the relaxation of initially segregated scalar mixtures in randomly stirred media, aiming to describe the overall concentration distribution of the mixture, its shape and rate of deformation as it evolves towards uniformity. A stirred scalar mixture can be viewed as a collection of stretched sheets, possibly interacting with each other. We consider a situation in which the interaction between the sheets is enforced by confinement and is the key factor ruling its evolution. It consists of following a mixture relaxing towards uniformity around a fixed average concentration while flowing along a constant cross-section channel. The interaction between the sheets is found to be of a random addition nature in concentration space, leading to concentration distributions that are stable by self-convolution. The resulting scalar field is naturally coarsened at a scale much larger than the dissipation scale. Consequences on the mixture entropy and scalar rate of dissipation are also examined.

1. Introduction

Stirring motions in deformable media such as fluids distort material lines and increase their length. A scalar blob is, generically in an incompressible medium, stretched in one direction and compressed in the other, the underlying motions being either persistent, smooth and time-dependent (chaotic) or turbulent. The blob's resulting topology is that of a convoluted sheet in three dimensions. For a diffusive scalar the kinematics of the flow affects the resulting convection–diffusion problem and defines the mixing time t_s (see Appendix A). Beyond that time, the sheet has a transverse width $s(t_s)$ which remains constant or re-increases slowly, equilibrating diffusive broadening and substrate compression, while its stretched dimensions continue to expand.

Let us take the simple example of a blob of initial size s_0, stirred in two dimensions by a constant stretching rate γ (see Appendix A). The length of the blob is $\ell(t) = s_0\,\mathrm{e}^{\gamma t}$ and, after the mixing time $t_s = (1/2\gamma)\ln(\gamma s_0^2/D)$ in which D is the scalar diffusivity, it has the shape of a lamella whose transverse width is $s(t_s) = \sqrt{D/\gamma}$. The net surface area $A(t)$ of the lamella is thus

$$A(t) = s_0\sqrt{D/\gamma}\,\mathrm{e}^{\gamma t}. \tag{1.1}$$

If the stirring protocol occurs on a finite size domain with fixed area A_0, it is clear that as soon as $A(t) > A_0$, some stretched/folded parts of the lamella will have to overlap and merge. The phenomenon is for example obvious in figures 1 and 5. From that instant of time, the resulting mixture cannot be viewed as a set of independent pieces of lamellae, and the interaction between these pieces has to be accounted for

† Also at Institut Universitaire de France.

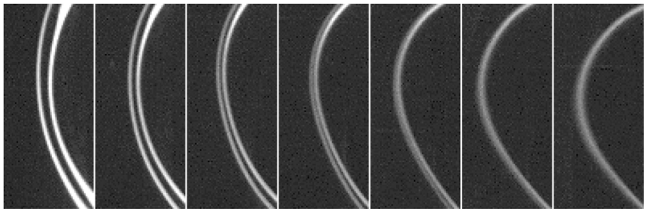

FIGURE 1. Close-up of the merging process of two nearby sheets in a set-up similar to that of figure 2.

to understand the fate of the overall mixture. Owing to the linearity of the Fourier diffusion equation, the concentration profile of any blob of size s_0 is obtained by a summation of the impulse response of the diffusion equation $(C_0 \mathrm{d}\xi/2\sqrt{\pi\tau})\,\mathrm{e}^{-\xi^2/4\tau}$ over the initial width of support (i.e. $\{-s_0/2, s_0/2\}$ in one dimension) as (Fourier 1822 and Appendix A)

$$C(\xi,\tau) = \int_{-1/2}^{1/2} \frac{C_0 \mathrm{d}\xi'}{2\sqrt{\pi\tau}}\,\mathrm{e}^{-(\xi-\xi')^2/4\tau}. \tag{1.2}$$

The concentration profile of a set of two lamellae such as those shown in figure 1, respectively characterized by profiles $C_1(\xi,\tau)$ and $C_2(\xi,\tau)$, is thus obtained by the summation

$$C(\xi,\tau) = C_1(\xi,\tau) + C_2(\xi,\tau). \tag{1.3}$$

The elementary composition rule of (1.3) is the building block of the evolution of a complex mixture.

A further indication of the nature of the interaction is given by considering the scalar field resulting from the merging of two independent scalar plumes.

1.1. *Interacting plumes and composition rule*

Consider two scalar sources, independent of each other and separated by a distance of the order of the integral scale of the flow L, merging in a turbulent medium as shown in figure 2. Let $P_1(C)$ and $P_2(C)$ be the elementary histograms of each of the two sources at one point in the flow obtained, for instance by switching one of the sources on while the other is off and vice versa, and let $P_{1+2}(C)$ be the compound histogram at that same location as illustrated in figure 3. As long as the plumes emanating from each of the sources do not interfere, the sources develop in an anti-correlated manner: the concentration measurement point is either in one plume or in the other, and the compound histogram is simply the weighted sum of the original ones (see also Warhaft 1984). Then, as soon as the plumes merge, it is experimentally observed that $P_{1+2}(C)$ is very close to the *convolution* of $P_1(C)$ and $P_2(C)$. In other words, the concentration C in a region of a flow is the sum of the concentrations C_1 from plume 1 and C_2 from plume 2 in the same region, C_1 and C_2 being chosen 'independently' in each of the original distributions provided that $C = C_1 + C_2$. This fundamental observation is written

$$P(C) = \int_0^C P_1(C_1) P_2(C_2)\,\mathrm{d}C_1, \tag{1.4}$$

where $C = C_1 + C_2$. The same observation is made by dividing a single plume in two, each sub-plume being marked with a different colour.

FIGURE 2. Two sources discharging in a turbulent medium in which they mix. Their separation is of the order of the local integral scale L.

1.2. *Compound plume*

A coherent compound plume is realized by injecting two different scalars through two nearby tubes of diameter $d \ll L$, as seen in figure 4. Planar measurements of the fluorescent scalar field are obtained by shining a plane mono-mode (488 nm) Argon laser sheet through the water tank in a plane containing the axis of the mean flow. A 768×1024 wide 3-CCD camera at 10 bits per pixel images the field. As opposed to the case presented above, the two scalars are initially injected at the same location in the main jet, where they are subjected to strongly correlated motions.

The resulting distributions are shown in figure 4. The global scalar field of the 'super' stream (obtained by deliberately making indiscernible the red and the green) is made up of the independent contribution of two elementary streams (the red and the green). Although injected nearly at the same location in the flow and thus subjected to similar histories at the beginning, fluid particles from the green stream are independent from those coming from the red stream at $x/d = 30$. Since the distinction between red and green particles was made arbitrarily in these experiments, it can be concluded that a single plume is the result of the random superposition of smaller plumes. The same experiments have been done using a coaxial jet, with the same results.

The random interaction rule in (1.4) was first proposed in a related manner by Curl (1963) and since then has been referred to as the celebrated 'coalescence–redispersion' model: particles meet at random, and as they coalesce their concentration levels are equalized before breaking up to meet other particles in a sequential fashion. A very similar construction was imagined by von Smoluchowski (1917) to represent the

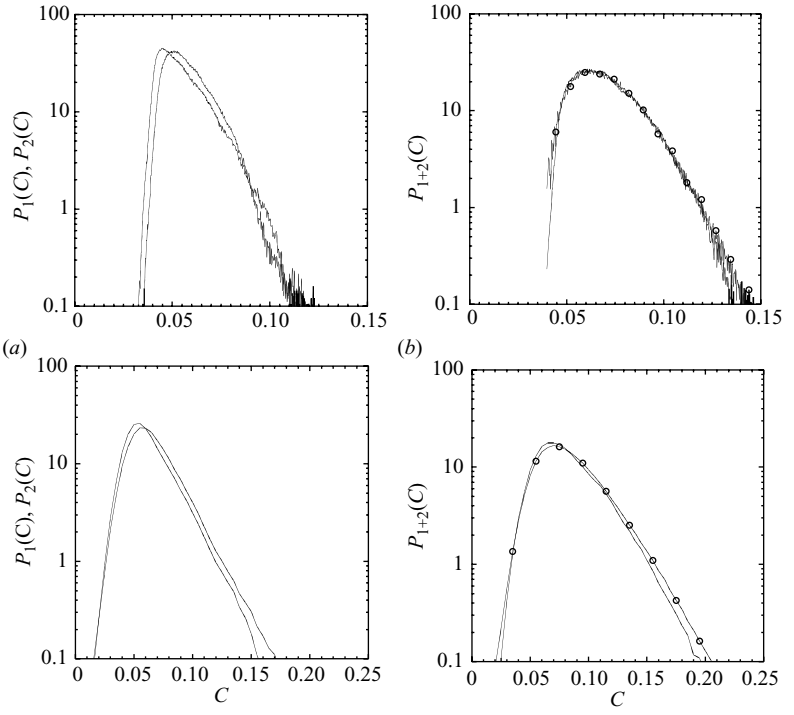

FIGURE 3. Composition of sources of heat (top; $Sc = 7$, $x/d = 12$) and fluorescein (bottom, $Sc = 2000$; $x/d = 13$) in water in a set-up like the one of figure 2. (*a*) Distributions of the bare sources $P_1(C)$ and $P_2(C)$. (*b*) Reconstruction of the scalar field from $P_1(C)$ and $P_2(C)$ by convolution (circles) and comparison with the actual distribution $P_{1+2}(C)$ in the presence of two sources (solid line).

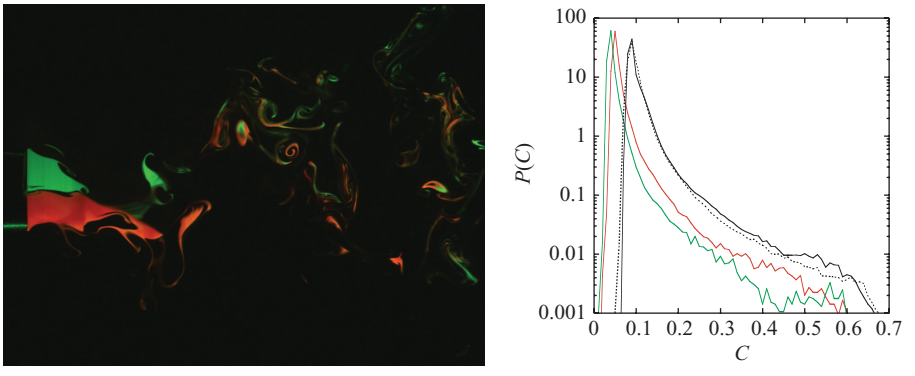

FIGURE 4. (*a*) A compound plume made of rhodamine (red) and fluorescein (green), injected by two identical nearby tubes of diameter $d = 8$ mm. (*b*) Concentration distributions of a rhodamine stream (red) and fluorescein stream (green) recorded at a distance $x/d = 30$ from the injection location and resulting distribution of the whole scalar field making no distinction between both scalars (black) compared to the one expected from a pure independence of the two fields (dotted line), namely the convolution operation of (1.4).

kinetic aggregation of colloidal particles and the distribution of the particle cluster sizes. Pumir, Shraiman & Siggia (1991) have, in a slightly different context, developed the same ideawhich leads to an evolution principle for $P(C, t)$ based on its convolution

with itself, reflecting the random addition of the scalar levels C in the mixture. Villermaux & Duplat (2003) have further suggested that the composition of random mixtures could be represented along these lines, and provided some experimental evidence and a kinetic equation for $P(C, t)$ (see also Venaille & Sommeria 2007). The present work makes this point of view more precise, presents new experimental evidence and documents some of its consequences.

2. Mixing in a confined environment

2.1. *Square channel flow*

A turbulent jet of water plus diluted fluorescein discharges in a square transparent long duct. The jet and the duct are immersed in a large tank filled with water at rest. The jet exit velocity u is such that $Re = ud/\nu \simeq 10^4$ with a turbulence intensity u'/u about 8% in that case (Schlichting 1987). For a given duct cross-section, the injection diameter d and the velocity of the co-flow at the entrance of the duct can be varied so that the average concentration of the dye in the channel $\langle C \rangle$ can be set at will. Since the cross-section of the duct and the average velocity of the mixture in the downstream direction are constant, the average concentration is conserved. The experiments presented here have been done with $d = 8\,\text{mm}$ and a square ($L \times L$ with $L = 3\,\text{cm}$) duct. Planar measurements of the fluorescent scalar field were obtained by shining a plane mono-mode (488 nm) argon laser sheet through the water tank in a plane containing the axis of the mean flow. The images were recorded by a cooled 12 bits 1280×1024 pixels wide CCD camera.

As can be seen in figure 5, the dye rapidly invades the whole cross-section of the duct, and its concentration differences are progressively erased while travelling downstream to relax towards a more or less uniform mixture. After the dye has filled the channel cross-section and evolved around a constant average concentration, the distribution $P(C)$ presents a skewed bell-like shape which gets narrower around $\langle C \rangle$ in time. Axial distances x are converted to time t through the average axial velocity u with confidence, as it is known that radial velocity profiles in a turbulent duct are flat ($u'/u \approx 0.08$; see Schlichting 1987) so that

$$x = u\,t. \tag{2.1}$$

As shown in figure 6, the shape of $P(C)$ is very well described by a family of one-parameter distributions, namely gamma distributions of the form

$$P(X = C/\langle C \rangle) = \frac{n^n}{\Gamma(n)}\, X^{n-1}\, \mathrm{e}^{-nX}. \tag{2.2}$$

The parameter n is adjusted at each downstream location for the gamma distribution of (2.2) to fit the experimental one. It is seen in figure 6 that the fairness of the fit holds for the whole concentration range, down to low probability levels, and accounts for the downstream deformation of $P(C)$ through the single parameter n, whose dependence on the downstream location is quite strong: figure 6 suggests a power-law type of dependence with an exponent between 2 and 3; the line drawn has a slope 5/2. The dependence of n on the jet Reynolds number is, if noticeable, very weak, when Re is varied by a factor 2, as noted in Villermaux & Duplat (2003).

3. Self-convolution processes

As they are brought together in the flow, scalar sheets interpenetrate to give rise to new sheets whose concentration profile is the *addition* of the original ones

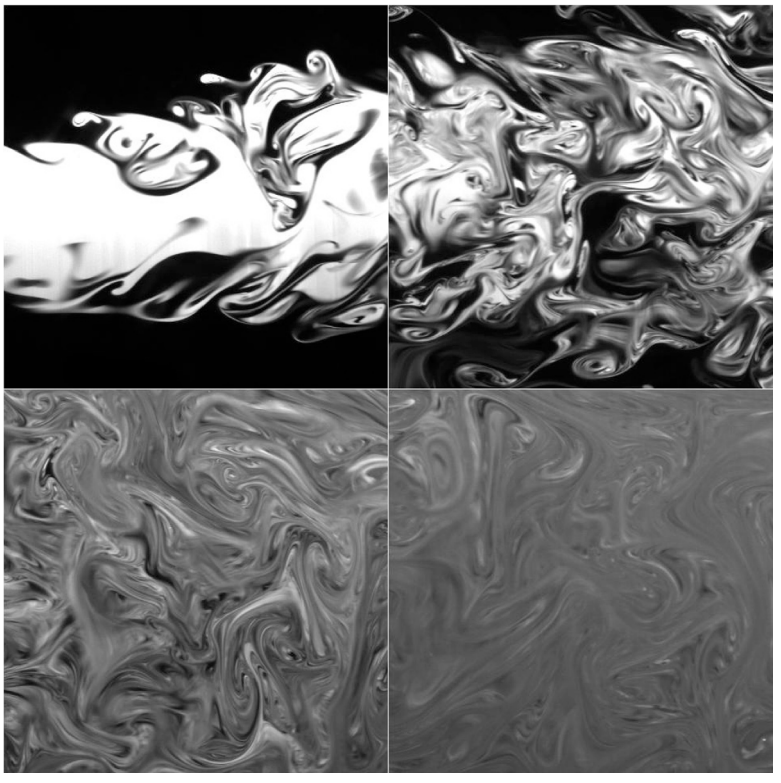

FIGURE 5. Mixing of a dye discharging from a jet of diameter $d = 8\,\mathrm{mm}$ in a square ($L \times L$ with $L = 3\,\mathrm{cm}$) duct. From 1 to 4, successive instantaneous planar cuts of the scalar field at increasing downstream locations in the duct, showing the progressive uniformization of the dye concentration levels.

(figure 1). This elementary interaction rule, that is the addition, is a consequence of the linearity of the Fourier diffusion equation. We show below how this rule, plus an additional assumption on the nature of the interactions in the flow, implies a kinetic evolution equation for the distribution of the concentration levels $P(C, t)$ as time progresses.

3.1. *Detailed process*

We conjecture that the impact of turbulence on the process is to make the additions of the concentration levels in the flow *at random*; this is in fact the only feature on which we need to proceed, and this feature completely characterizes the nature of the mixture evolution in a particular limit at least. In the following, a concentration level C means the 'maximal' concentration $C(0, t)$ across a given sheet, and we disregard the contribution of the intermediate levels of the spatial profile $C(z, t)$ to the global distribution $P(C)$; this is justified as soon as $t > t_s$ (a discussion of which can be found in Meunier & Villermaux 2003; see also Appendix A). Since the concentration levels C each sheet carries are random variables, the addition of these variables translates, in the probability density function space $P(C)$, in a *convolution*. There are in fact many different ways to represent this process; we single out two extremes (see also figure 7) before giving the general formulation. Let the merging rate of two nearby

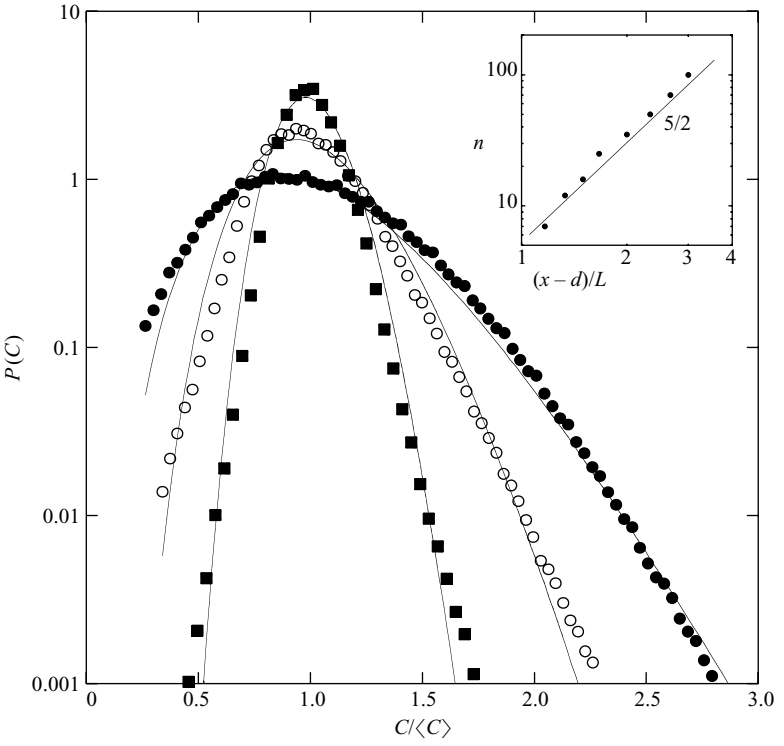

FIGURE 6. Downstream evolution of the concentration distribution $P(C)$ as the dye progresses along the duct as shown in figure 5. The concentration distribution of the evolving mixture gets narrower around the average concentration $\langle C\rangle = 0.3$. Solid line: experimental distributions. Broken line: distributions given by (2.2). Insert: fitting parameter n of the distribution (2.2) as a function of the downstream distance $(x-d)/L = 1$ (●), 1.5 (○), 2.5 (■). $Re = 4 \times 10^3$.

sheets be r:

(i) First, one can imagine that at time t, a fraction ϵ of the sheets in the flow volume undergoes a complete addition with its neighbours, the other fraction $1-\epsilon$ being left unchanged with respect to this addition process because those sheets of which it was a part had no neighbours at that instant of time. Thus, the distribution $P(C, t+\delta t)$ at time $t+\delta t$ will be such that

$$P(C, t+\delta t) = \epsilon P^{\otimes 2}(C, t) + (1-\epsilon)P(C, t), \tag{3.1}$$

where $P^{\otimes 2}(C, t) = P(C, t) \otimes P(C, t)$ stands for the self-convolution of $P(C, t)$, as defined in (1.4) and where

$$\epsilon = r\delta t. \tag{3.2}$$

It is useful to consider the Laplace transform of $P(C)$, which conveniently transforms convolution products into simple products

$$\tilde{P}(s) = \int_0^\infty P(C)\, \mathrm{e}^{-sC}\, \mathrm{d}C, \tag{3.3}$$

and rewrite (3.1) in the differential limit $r\delta t \to 0$ as

$$\partial_t \tilde{P} = r(-\tilde{P} + \tilde{P}^2), \tag{3.4}$$

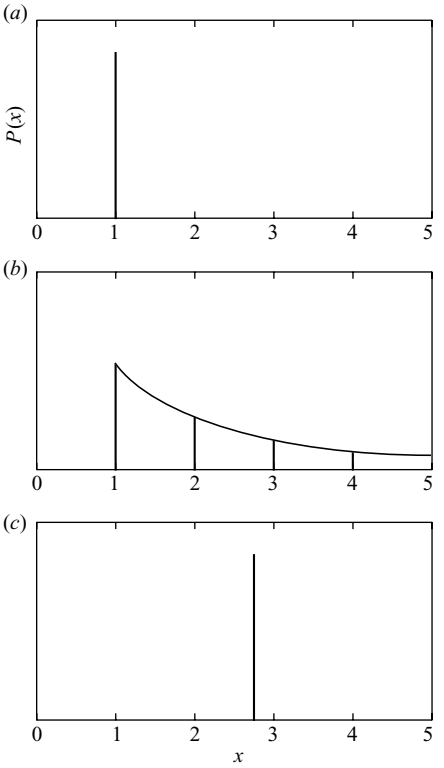

FIGURE 7. Self-convolution processes: illustration of the two extreme routes of (3.4) and (3.7) for the initial condition $P(x, t=0)=\delta(x-1)$ shown in (a). The complete convolution on a discrete time scale route $\partial_t \tilde{P} = r(-\tilde{P} + \tilde{P}^2)$ is shown in (b) to give rise for $P(x, t)$ to a series of Dirac deltas at integer values of x with an exponentially decaying envelope $\mathrm{e}^{-x/\mathrm{e}^{rt}}/\mathrm{e}^{rt}$. Convolution on a continuous time scale $\partial_t \tilde{P} = r\tilde{P} \ln \tilde{P}$ translates, as shown in (c), the initial condition on the x-axis such that $P(x, t)=\delta(x-\mathrm{e}^{rt})$.

an equation familiar in the context of kinetic aggregation since von Smoluchowski (1917) and whose asymptotic solution is the decaying exponential

$$P(C, t) \sim \exp\left(-\frac{C}{\mathrm{e}^{\int_0^t r\mathrm{d}t'}}\right). \tag{3.5}$$

This defines a particular route for the evolution of $P(C)$, made up of an intermittent sequence of complete convolutions on a 'discrete' time scale δt: a small fraction of the sheets in the flow undergo a complete addition from step to step.

(ii) Another way to represent the self-convolution process directing the evolution of $P(C)$ is to assume that the convolution operation occurs on a 'continuous' time scale everywhere in the flow, with all sheets merging with their neighbours in a continuous way, therefore altering the distribution $P(C)$ even on an infinitesimal time scale. In that case, the equivalent of (3.1) written for the evolution for the Laplace transform of $P(C)$ is

$$\tilde{P}(s, t+\delta t) = \tilde{P}^{1+\epsilon}(s, t) = \tilde{P}(s, t)\exp(\epsilon \ln \tilde{P}(s, t)). \tag{3.6}$$

Writing $\mathrm{e}^{\epsilon \ln \tilde{P}(s,t)} \approx 1 + \epsilon \ln \tilde{P}(s, t)$ in the differential limit $\epsilon = r\delta t \to 0$, (3.6) leads to

$$\partial_t \tilde{P} = r\tilde{P} \ln \tilde{P}, \tag{3.7}$$

whose solution obviously leads to a true self-convolution of the initial distribution $P(C, t=0)$ as

$$P(C,t) = P(C,t=0)^{\otimes \exp(\int_0^t r\,\mathrm{d}t')}, \tag{3.8}$$

with no universal asymptotic shape (see also Venaille & Sommeria 2007). This defines another route for the evolution of $P(C)$, made up of a continuous convoluted process: all sheets undergo additions continuously, everywhere in the flow.

The above two routes appear as two distinct limits of the more general evolution equation

$$\partial_t P = rn\left(-P + P^{\otimes 1+1/n}\right), \tag{3.9}$$

expressing the self-convolution of $P \equiv P(C,t)$ within a one-parameter equation whose solutions define a 'unique' family of distributions, parameterized by the unique parameter n. One recovers the intermittent sequence with discrete time of (3.1) with $n = 1$, and the progressive uniform process continuous in time of (3.7) is recovered with $n \to \infty$.

3.2. *The Liouville term and the general kinetic equations*

Concomitant to the addition process which alters its shape as time progresses, the change of $P(C,t)$ is also due to the trivial decay of C due to stretching: this results in a global shift of $P(C,t)$ towards lower concentration levels through the mass conservation balance

$$P(C+\delta C, t+\delta t) = P(C,t), \tag{3.10}$$

in the absence of other effects altering the shape of the distribution, where δC is the decrement of concentration by stretching during the time interval δt. This contribution to the rate of change $\partial_t P(C,t)$ is the familiar Liouville term

$$-\frac{\partial}{\partial C}\left(\left\langle \frac{\delta C}{\delta t}\right\rangle P\right) = \gamma \frac{\partial}{\partial C}(CP), \tag{3.11}$$

where the decrement

$$\left\langle \frac{\delta C}{\delta t}\right\rangle = -\gamma(t) C \tag{3.12}$$

defines $\gamma(t)$ and depends on the particular type of substrate deformation. If for instance the concentration in the sheets is such that $C \sim (\sigma t)^{-\beta-1/2}$, then $\gamma(t) = (\beta + 1/2)/t$. This global shift contributes, in all cases, in an additive manner to the overall rate of change of $P(C,t)$ owing, again, to the linearity of the microscopic diffusion equation.

3.2.1. *Mixtures with conserved average concentration*

Adding the Liouville global shift to the convolution contribution results in the overall mixture equation, describing its concentration content as a function of time

$$\partial_t P = \gamma\, \partial_C (CP) + rn\left(-P + P^{\otimes 1+1/n}\right), \tag{3.13}$$

whose version in the Laplace space reads

$$\partial_t \tilde{P} = -\gamma s \partial_s \tilde{P} + rn\left(-\tilde{P} + \tilde{P}^{1+1/n}\right). \tag{3.14}$$

From the chain rule giving the qth moment of the concentration distribution from its Laplace transform $\langle C^q \rangle = (-1)^q \partial^q \tilde{P}/\partial s^q|_{s=0}$ and remembering that $\tilde{P}(s=0,t)=1$ because $P(C,t)$ is a normed density probability function, one readily checks that the

average concentration $\langle C\rangle = -\partial\tilde{P}/\partial s|_{s=0}$ is conserved when the damping Liouville factor balances exactly the increase of concentration with sheet coalescence, i.e. when

$$\gamma = r. \tag{3.15}$$

With the above condition fulfilled, (3.14) is the expansion for large n of

$$\partial_t \tilde{P}(s,t) = \gamma n \left(-\tilde{P}(s,t) + \tilde{P}\left(\frac{s}{1+1/n}, t\right)^{1+1/n} \right), \tag{3.16}$$

which is the Curl's evolution equation (written in Laplace space) generalized to arbitrary n, the strict Curl's equation corresponding to $n=1$ (Curl 1963).

The structure of the kinetic equation (3.14) with $\gamma = r$ is such that the average concentration is conserved whatever the value of n, with no constraint or link with the parameter which contains the information on the stirring strength of the flow, that is the stretching rate γ. However, stretching and merging of the sheets are intimately linked. It is *because* the sheets are stretched that their concentration decreases and also *because* they are stretched that they are brought together and merge. It is thus natural to relate n to γ by

$$\frac{\mathrm{d}n}{\mathrm{d}t} = \gamma n. \tag{3.17}$$

Setting $\mathrm{d}n/\mathrm{d}t = \dot{n}$, the asymptotic solution to (3.14) is found by making use of the following transformations (see e.g. Friedlander & Wang 1966):

$$\left.\begin{aligned} P(C,t) &= \frac{1}{\langle C\rangle} F(\eta,\tau), \\ \eta &= \frac{C}{\langle C\rangle}, \\ \tau &= t, \end{aligned}\right\} \tag{3.18}$$

where $\langle C\rangle$ is the conserved average concentration. This is most conveniently done with the Laplace transform $\tilde{P}(s,t)$ defined in (3.3) for which the transformations in (3.18) are such that

$$\tilde{P}(s,t) = \tilde{F}(s',\tau) \quad \text{with} \quad s' = \langle C\rangle s, \tag{3.19}$$

where $\tilde{F}(s',\tau)$ is the Laplace transform of $F(\eta,\tau)$ in η. Noting that

$$s\frac{\partial\tilde{P}}{\partial s} = s\frac{\partial\tilde{F}}{\partial s'}\frac{\partial\tilde{s}'}{\partial s} = s\langle C\rangle\frac{\partial\tilde{F}}{\partial s'} = s'\frac{\partial\tilde{F}}{\partial s'}, \tag{3.20}$$

the scaled distribution $F(s',\tau)$ finally obeys

$$\partial_\tau \tilde{F} + \gamma s'\partial_{s'}\tilde{F} + = \dot{n}\left(-\tilde{F} + \tilde{F}^{1+1/n}\right). \tag{3.21}$$

The only place where τ explicitly enters into (3.21) is the term $\partial_\tau\tilde{F}$. Looking for a self-preserving solution to (3.21) independent of time and solely a function of $C/\langle C\rangle$ and n and remembering that $\dot{n} = \gamma n$, we seek a solution to

$$s'\partial_{s'}\tilde{F} = n\left(-\tilde{F} + \tilde{F}^{1+1/n}\right), \tag{3.22}$$

which is

$$\tilde{F} = \left(1 + \frac{s'}{n}\right)^{-n}, \tag{3.23}$$

thus, together with $n = \exp\int_0^t \gamma(t')\,\mathrm{d}t'$, solving the search for the full concentration distribution $P(C,t)$. Indeed, the inverse Laplace transform of (3.23), with $s' = \langle C\rangle s$,

is a *gamma* distribution of order n and average $\langle C\rangle$:

$$P(X = C/\langle C\rangle) = \frac{n^n}{\Gamma(n)}\, X^{n-1}\, \mathrm{e}^{-nX}. \tag{3.24}$$

This distribution was found to closely fit the experimental distribution of the mixture confined in a channel in § 2. These experiments have also revealed the time dependence of order n, which can now be understood by the coalescence process giving birth to the distribution (3.24): although the concentration of each individual element $C \equiv C(0, t)$ decreases in time because of stretching, the average concentration of the mixture $\langle C\rangle$ is conserved. This is so if the coalescence rate balances the Liouville damping factor. The piling-up of the concentration levels by coalescence contributes to the increase of the average concentration by a factor given by (3.9), that is $\exp\{\int \mathrm{d}n/n\} = n$. The average concentration is thus conserved provided

$$n = \frac{1}{C(0, t)} \sim t^{\nu}, \tag{3.25}$$

where $\nu = 5/2$ (see Appendix A), from which one recovers the definition of n through $\dot{n}/n = \gamma$ and $\gamma = -\mathrm{d}\ln C(0, t)/\mathrm{d}t$. This is also consistent with the experimentally measured time dependence of n, reported in figure 6.

The parameter n is the *number of convolutions*, and its variation in time induces the rate of deformation of the concentration distribution.

3.3. *An alternative description*

The construction mechanism of the concentration distribution we have given above relies on random addition of concentration levels with a 'fixed' number of additions n at a given instant of time. We show now that the very same result for $P(C, t)$ can be interpreted in a dual form, where elementary sheets bearing a *fixed* concentration level solely dependent on time through stretching undergo random additions whose *number is distributed*.

We call $p_0(C, t)$ the distribution of concentration of a single isolated sheet. Suppose now that k of these sheets have merged to give rise to a bundle of concentration C, and suppose that the number k is itself distributed among different bundles with distribution $Q(k)$ at a given instant of time. Then the macroscopic probability distribution of the concentration levels in the bundles is

$$P(C, t) = \int_0^{\infty} \mathrm{d}k\, Q(k) p_0^{\otimes k}, \tag{3.26}$$

where the symbol $\otimes$ denotes, as before, convolution with respect to concentration. The distribution $Q(k)$ is that of the number of aggregations k. Let us, for example, model its evolution by the irreversible aggregation scenario with discrete time we have introduced before leading to an equation of type (3.1):

$$\partial_t Q(k) = Q(k)^{\otimes_k 2} - Q(k), \tag{3.27}$$

where $\otimes_k$ now denotes a convolution with respect to the number k. Inserting it into (3.26) gives

$$\partial_t P(C, t) = \int_0^{\infty} \mathrm{d}k\, \partial_t Q(k) p_0^{\otimes k} = \int_0^{\infty} \mathrm{d}k (Q(k)^{\otimes_k 2} - Q(k)) p_0^{\otimes k}, \tag{3.28}$$

which we rewrite by splitting k into k_1 and k_2 and expressing the convolution integral on $Q(k)$ as

$$\partial_t P(C,t) = \int_0^\infty \mathrm{d}k_1 \mathrm{d}k_2 Q(k_1) Q(k_2) p_0^{\otimes k_1} \otimes p_0^{\otimes k_2} - P(C,t), \tag{3.29}$$

which can be further rearranged by separating the variables of integration as

$$\partial_t P(C,t) = \left(\int_0^\infty \mathrm{d}k_1 Q(k_1) p_0^{\otimes k_1} \right) \otimes \left(\int_0^\infty \mathrm{d}k_2 Q(k_2) p_0^{\otimes k_2} \right) - P(C,t), \tag{3.30}$$

giving finally

$$\partial_t P(C,t) = P(C,t)^{\otimes 2} - P(C,t), \tag{3.31}$$

actually coinciding with the expected evolution equation for $P(C,t)$ itself, which is characteristic of an aggregation process with discrete time but now derives from the distribution of the number of sheets that have aggregated.

4. Consequences

The detailed knowledge of the mixture's concentration distributions allows us to examine *a posteriori* some quantities which are usually modelled, or inferred, using additional hypotheses.

4.1. *Coarse-grained scale*

There are several physical length scales naturally involved in a stirred mixture. First, without stirring, that is in the pure diffusion limit on a still substrate, an obvious spatial scale is the initial size s_0 of the blob deposited in the medium. The concentration in the blob is appreciably decayed from its initial value when the blob is smeared by diffusion, that is when its current radius $\sqrt{Dt}$ is appreciably larger than s_0, and this of course happens when $t \gg s_0^2/D$. With stretching, the picture is substantially altered.

4.1.1. *Local dissipation scales*

Diffusive smearing is hastened in the presence of stirring because the scalar gradient is constantly steepened by the stretching. This, in turn, also alters the characteristic scale of the field itself. When the stretching of material surfaces is algebraic in time for instance, that is when $s(t) = s_0(1+\sigma t)^{-\beta}$ with β some positive exponent, the concentration gradient at the mixing time spans a typical distance of the order of

$$s(t_s) \sim s_0(\sigma t_s)^{-\beta} = s_0 Pe^{-\beta/(2\beta+1)} \ll s_0 \quad \text{when} \quad Pe = \frac{\sigma s_0^2}{D} \gg 1 \tag{4.1}$$

after re-increasing like $\sqrt{Dt}$ because the rate of stretch diminishes in time like $\gamma \sim 1/t$. This scale also sets the width of an isolated blob dissipating in the medium. If the rate of stretch γ is constant in time, then the typical size of the scalar gradient which 'dissipates' the scalar differences equals

$$s(t_s) \sim s_0 \, \mathrm{e}^{-\gamma t_s} = \sqrt{\frac{D}{\gamma}}, \tag{4.2}$$

usually called the Batchelor scale after Batchelor (1959). The above scales are obtained by balancing the rate of compression $\gamma(t) = \mathrm{d}\ln s(t)/\mathrm{d}t$ with the diffusive rate of broadening $D/s(t)^2$. The same procedure can be further generalized to a stretching,

or compression, rate $\gamma(s)$ which is constant in time but depends on the separation distance s. Choosing for instance $\gamma(s) \sim (\epsilon s)^{1/3}/s$, as sometimes invoked in high-Reynolds-number turbulent flows (Frisch 1995), the corresponding 'dissipation scale' equilibrating substrate compression and diffusive broadening is

$$\left(\frac{D^3}{\varepsilon}\right)^{1/4}, \tag{4.3}$$

where ε stands for the rate of dissipation of mechanical energy per unit mass in the flow, a scale usually referred to as the Corrsin–Obukhov length scale (after Corrsin 1951 and Obukhov 1949).

Let us also mention that this local equilibrium paradigm applies beyond the scalar mixing context and is successful at describing the aspect ratio of drops immersed in a non-miscible sheared substrate (Stone 1994) or the maximal size of drops and bubbles in a turbulent flow (Clay 1940; Hinze 1955) by an appropriate balance between hydrodynamics stresses and capillary restoration forces at the scale of the drops themselves.

4.1.2. *The coarse-grained scale*

All the above scales describe the size of an *isolated* object arising from the 'local' balance between a time characteristic of the motions in the underlying substrate and a diffusion time. However, we have shown how the global concentration content of a stirred mixture results from the merging of *nearby* objects, namely scalar sheets, which interact through a *random aggregation* process. This phenomenon has an effect on some geometrical facets of the mixture. In particular, we show below that the concentration field C of the mixture is smooth on a scale which is much larger than the typical scale of its gradient estimated from the above length scales and that this *coarse-grained* scale directly reflects the aggregation construction of the concentration field.

We denote as $V_>(r)$ the variance of the concentration field coarse-grained at scale r. If $F(k)$ is its spectrum, then

$$V_>(r) = \int_{2\pi/L}^{2\pi/r} F(k)\,\mathrm{d}k. \tag{4.4}$$

Equivalently, $V_>(r)$ can be computed by filtering the original concentration field $C(x)$ with a top-hat window of width r defining a coarse-grained field $C_r = C(x) \otimes H_r(x)$ with $H_r(x)$ equal to $1/r$ for $0 < x < r$ and equal to 0 for $x > r$. Then

$$V_>(r) = \langle (C_r - \langle C_r \rangle)^2 \rangle. \tag{4.5}$$

We have used definition (4.5) to compute $V_>(r)$ from the experimental concentration signals. The operation is shown visually in figure 8. The dependence of $V_>(r)$ on r is shown in figure 9 for different injection and stirring conditions. The coarse-grained variance presents an inverted S shape, which shares some of its features with $P(C)$ itself: it is independent of the Reynolds number Re and is shifted by varying the diffusivity of the scalar measured by Sc. It is, however, independent of the scalar injection scale d. Half of the variance has been erased by coarse-graining the field up to the scale $r = \eta$, which coincides approximately with the location of the S-shaped inflection point. All measurements for different scalars and flows are reported in figure 10. They are consistent with

$$\eta = LSc^{-2/5}. \tag{4.6}$$

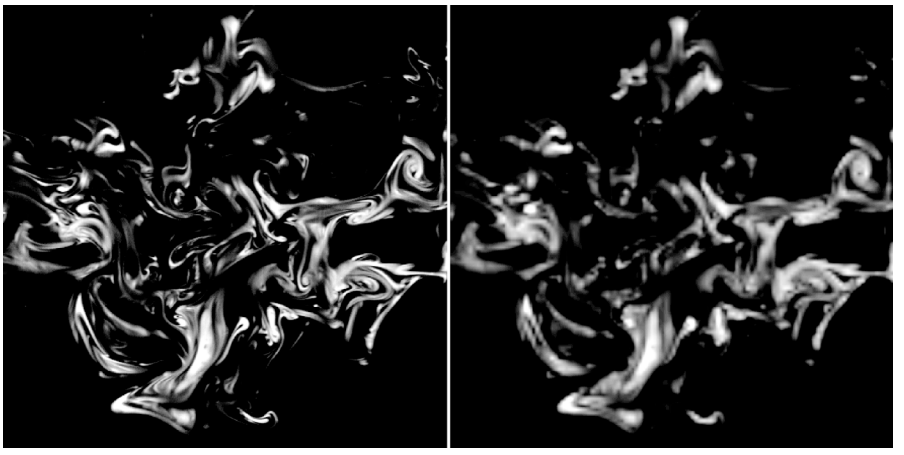

FIGURE 8. Coarse-graining operation of the scalar field. The field has been coarse-grained up to the scale η.

The *coarse-grained scale* η solely depends on the large stirring scale of the flow and on the diffusional properties of the scalar. This is the minimal 'scale of scrutiny' devised by Danckwerts (1953) to describe a mixture. We explain its origin below.

4.1.3. *Aggregation of a bundle of sheets*

We do not consider any more an isolated scalar sheet being stretched but instead a bundle of parallel sheets in the process of merging into each other under the action of a large-scale stretching rate. As outlined earlier, this process is the one occurring permanently in a stirred mixture and which gives rise, in the confined case in particular, to the self-convoluting construction of the concentration distribution.

We will consider that the sheets are stretched in two directions parallel to their plane under the action of an elongation rate σ, identical in the two directions, constant in time and uniform over a scale L. We choose a simple initial scalar field $C(x, t=0)$ consisting of a bundle of parallel sheets, each separated from its immediate neighbours by a distance $2\pi/k_0$ and piled up over a distance of the order of L. The sheets are compressed in the direction parallel to their transverse size. We first disregard the distribution of the concentration levels between the sheets. A functional form for $C(x, t=0)$ having the required features is

$$C(x, t=0) = 1 + \cos(k_0 x) \quad \text{for} \quad -L/2 < x < L/2 \tag{4.7}$$

and equal to 0 elsewhere. The convection diffusion equation

$$\frac{\partial C}{\partial t} + \gamma(t) z \frac{\partial C}{\partial z} = D \frac{\partial^2 C}{\partial z^2} \tag{4.8}$$

with $\gamma(t) = \mathrm{d} \ln s(t)/\mathrm{d}t$ is transformed in a pure diffusion equation by the same space and time transformation as the ones used in Appendix A. It is solved with $s(t)/s_0 = 1/(1+\sigma t)^2$ to give the concentration field at any time as

$$C(x, t) = 1 + \cos(\xi)\, \mathrm{e}^{-\tau} \tag{4.9}$$

with

$$\xi = k_0 x (1+\sigma t)^2 \quad \text{and} \quad \tau = \frac{D k_0^2}{5\sigma}(-1 + (1+\sigma t)^5). \tag{4.10}$$

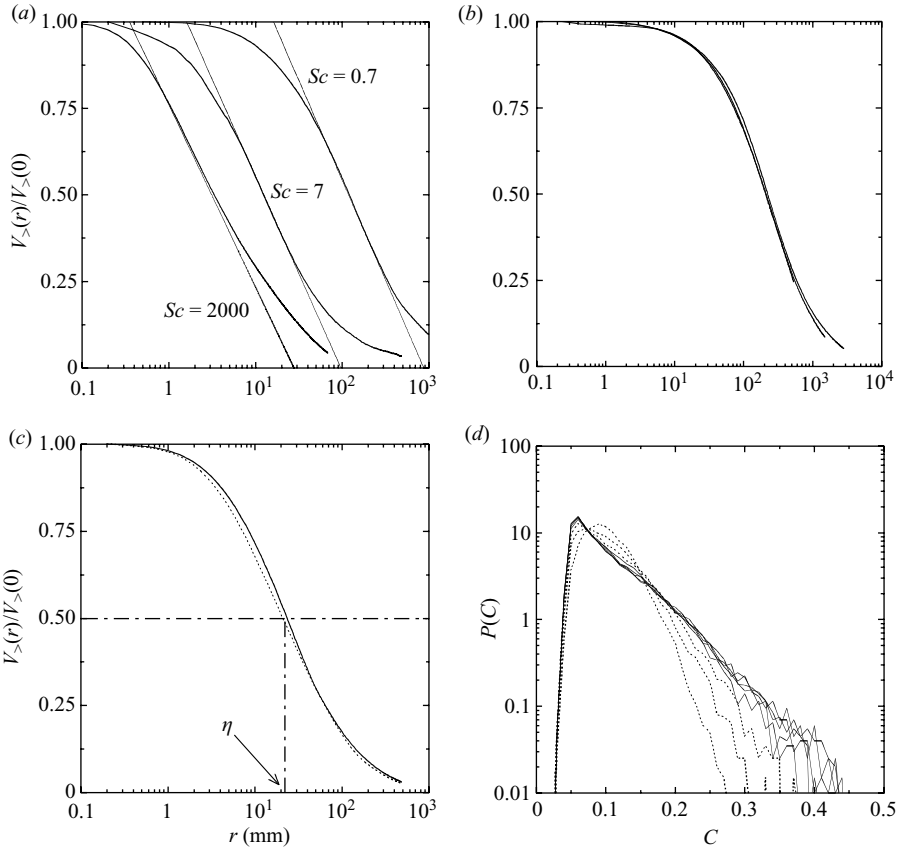

FIGURE 9. The coarse-grained variance of the concentration field $V_>(r)$ as a function of the coarse-grained distance r for different scalars and stirring conditions with $L = 6$ cm. (a) $V_>(r)$ versus r for three Schmidt numbers at a fixed location downstream of the scalar source. Half of the variance of the field has been erased by coarse graining at the scale $r = \eta$, which depends on Sc. (b) At a fixed location $x/d = 20$ downstream of a $d = 3.3$ cm source in air ($Sc = 0.7$) for $u = 3\,\mathrm{m\,s^{-1}}$ ($Re = 9000$), $u = 6.2\,\mathrm{m\,s^{-1}}$ ($Re = 19\,000$) and $u = 11.6\,\mathrm{m\,s^{-1}}$ ($Re = 35\,000$). The corresponding Corrsin–Obukhov length is $\eta_{\mathrm{CO}} = LRe^{-3/4}Sc^{-3/4} \approx 0.1$ mm. (c) At a fixed location $x/d = 12.5$ and $Sc = 7$ for $Re = 6000$ and two different injection diameters $d = 6$ mm (dotted line) and $d = 10$ mm (continuous line). The corresponding Batchelor length is $\eta_{\mathrm{B}} = LRe^{-3/4}Sc^{-1/2} \approx 0.03$ mm. (d) Change of the concentration distribution $P(C)$ as the coarse-graining scale is increased for $x/d = 10$, $Sc = 0.7$ and $Re = 45\,000$: $r = 2$ to 256 mm by factors of 2. There are five curves with $r < \eta$ and three with $r > \eta$ (dashed line).

The time needed to complete the coalescence of the sheets in the bundle is the time required to make the concentration modulations small compared to unity, that is to make the factor $\mathrm{e}^{-\tau}$ appreciably small (see (4.9)). This occurs from the instant of time making τ of order unity, defining again the mixing, or coalescence, time as

$$t_s \sim \frac{1}{\sigma} Pe^{1/5} \quad \text{with} \quad Pe = \frac{\sigma}{Dk_0^2} \gg 1. \tag{4.11}$$

At that instant of time, the concentration in the bundle of merged sheets is close to uniform, the modulations having been essentially erased. The transverse size of the bundle, initially equal to L, has decreased accordingly. It has been compressed by an amount $(1+\sigma t_s)^2 \approx Pe^{2/5}$ (see Appendix A). The transverse size of the bundle defining

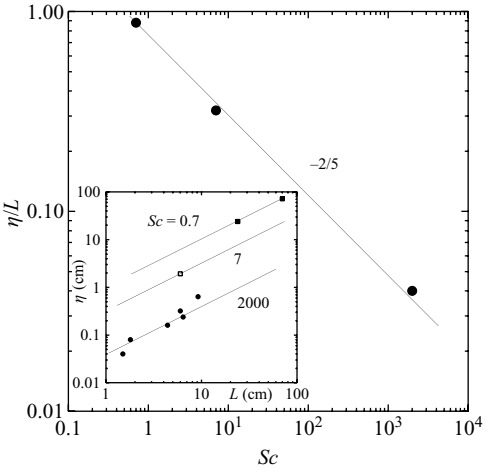

FIGURE 10. Coarsening scale η versus integral scale L measured for the flow conditions of figure 9, including a broad range of integral scales L and three different Schmidt numbers Sc. The insert shows that η is proportional to L (lines slopes being unity), and the figure suggests that $\eta = LSc^{-2/5}$ is consistent with the observed Schmidt number dependence of η.

a region of close-to-uniform concentration is thus

$$\eta = LPe^{-2/5}. \tag{4.12}$$

If finally k_0 is further set at $s_0^{-1} \sim \sqrt{\sigma/\nu}$, then $Pe = \sigma/Dk_0^2 = \nu/D = Sc$, and η coincides with the anticipated value given in (4.6).

This result is not contingent upon the particular choice made for the initial concentration profile in (4.7). If instead one considers a set of adjacent sheets of width s_0 with distributed initial concentrations, the spectrum of such a concentration field can be computed exactly as

$$F(k, t = 0) = \frac{\sigma_0^2}{\pi s_0 k^2}(1 - \cos(ks_0)), \tag{4.13}$$

if $\sigma_0^2 = V_>(0)$ is its initial variance. Making the change of variables

$$\hat{F}(k_\xi, \tau) = s(t)F(k_\xi/s(t), t(\tau)), \tag{4.14}$$

it is readily seen from the diffusive relaxation of the spectrum that the variance σ^2 at any later time is

$$\sigma^2 = \int_{-\infty}^{+\infty} \mathrm{d}k_\xi \hat{F}(k_\xi, \tau) = \int_{-\infty}^{+\infty} \mathrm{d}k_\xi \hat{F}(k_\xi, 0) \exp\left(-2k_\xi^2\tau\right), \tag{4.15}$$

that is

$$\frac{\sigma^2}{\sigma_0^2} = \frac{1}{\sqrt{\pi}\psi}\left(\mathrm{e}^{-\psi^2} - 1\right) + \mathrm{erf}(\psi) \tag{4.16}$$

with $\psi = 1/\sqrt{8\tau}$. The variance has been reduced by a factor close to 1/2, when $\psi = 1$, which is precisely the criterion used to define η. The analysis is readily generalized to the more realistic situation in which initial sheet thicknesses are distributed, as is the case in nature (see e.g. Schumacher, Sreenivasan & Yeung 2005).

The above mechanism showing the existence in the scalar field of a scale of the order of the large stirring scale is reminiscent of the ramp–cliff–plateau structures observed

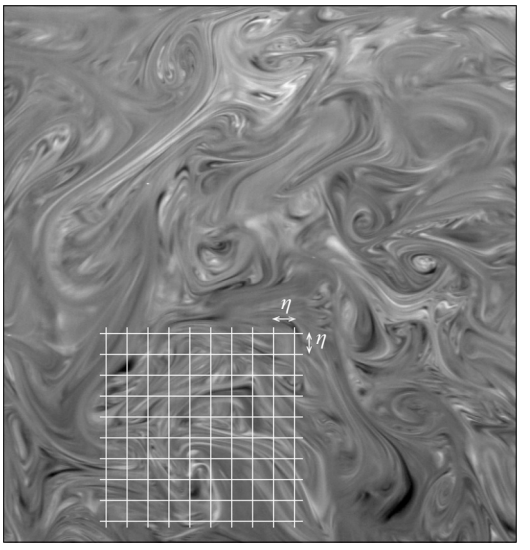

FIGURE 11. Definition sketch of a micro-state to compute the number of complexions w. There are k sheets of concentration $c(0, t)$ each per minimal coarse-graining cell of linear size η (artificially enlarged here), giving a coarse-grained concentration $C = kC(0, t)$.

long ago in shear flows. In it, L-wide regions of nearly uniform concentration are separated by steep cliffs absorbing a concentration difference of the order of the mean (Sreenivasan 1991; Holzer & Siggia 1994; Pumir 1994; Warhaft 2000). Villermaux & Duplat (2006) and Chertkov, Kolokolov & Lebedev (2007) have noted the possibly strong effect of weak molecular diffusion at large scales, invoking a mechanism similar to the one described here.

4.2. *Entropy*

The scalar field is composed of a number of elementary sheets which are nested in bundles of linear size η. This nesting operation defines, through the aggregation scenario described earlier, the macroscopic concentration levels C and their relative occurrence in the field $P(C)$. We wish now to compare this concentration distribution with the one which would be obtained from a purely random scatter of the sheets in space. We will therefore consider a closed system characterized by an invariant average concentration $\langle C \rangle$.

Let us thus consider a partition of space, consisting of N boxes of size η in which are scattered K elementary sheets as in figure 11. We call n_k the number of boxes bearing k sheets, and the average number of elements per box is $\langle k \rangle = K/N$. There are obviously a number of ways to realize a given partition $\{n_k\}$. Since the number of elementary sheets k in a box define the concentration C of that box, the number n_k is also the number of times the concentration C will be found in the field. The number of microscopic states leading to a given partition $\{n_k\}$ (see e.g. Mayer & Mayer 1966), and thus to a given realization of the macroscopic concentration distribution, is

$$w(\{n_k\}) = \frac{N!}{\prod_{k=0}^{K} n_k!} \cdot \frac{K!}{\prod_{k=0}^{K} (k!)^{n_k}}, \tag{4.17}$$

together with the conservation laws

$$\sum_{k=0}^{K} n_k = N \quad \text{and} \quad \sum_{k=0}^{K} k n_k = K. \tag{4.18}$$

The structure of (4.17) is as follows: The number of distinguishable arrangements in the set of the $\{n_k\}$ boxes into N boxes is $N!/\prod_k n_k!$, while any permutation of the k elements in a given box leads to the same macroscopic concentration, hence the factor $K!/\prod_k (k!)^{n_k}$. The number of microscopic states $w(\{n_k\})$ has a maximum for a particular partition $\{n_k\}$. We look for the maximum of $w(\{n_k\})$ by letting the values of n_k vary by an amount δn_k with the constraints $\delta K = \sum_k k\delta n_k = 0$ and $\delta N = \sum_k \delta n_k = 0$. Looking for the maximum of $w(\{n_k\})$ is equivalent to looking for the maximum of its logarithm; writing $\delta \ln w(\{n_k\}) = 0$ leads to

$$\sum_{k=0}^{K} \delta n_k \{-(\ln n_k + \ln k!) + \alpha k + \beta\} = 0, \tag{4.19}$$

where α and β are Lagrange multipliers, such that the conservation laws of (4.18) are fulfilled. The optimal distribution $p_k = n_k/N$ is a Poisson distribution

$$p_k = \frac{n_k}{N} = \frac{\langle k \rangle^k}{k!} \mathrm{e}^{-\langle k \rangle} \tag{4.20}$$

of parameter $\langle k \rangle$, the average number of elements per box. This is the distribution of the number of objects in a regular partition of space, when the objects are spread at random; it is, besides, readily obtained from binomial counting

$$p_k = \left(\frac{1}{N}\right)^k \left(1 - \frac{1}{N}\right)^{K-k} \frac{K!}{k!(K-k)!}, \tag{4.21}$$

in the limit in which the occupancy probability of one box by one sheet $1/N$ goes to zero (i.e. very large sample). This distribution is not uniform, but *tends towards* a uniform distribution centred on the mean $\langle k \rangle = K/N$ for $K \to \infty$ at fixed mean. It is sometimes encountered with low-inertia particles in turbulent flows (Eaton & Fessler 1994; Lei, Ackerson & Tong 2001). Since each elementary sheet has a concentration $C(0,t)$, each of the n_k coarse-grained boxes has a macroscopic concentration $C \sim kC(0,t)$. The distribution of the number of objects per coarse-graining scale of (4.20) thus gives rise to a macroscopic concentration distribution $P_E(C)$ given by

$$P_E(X = C/\langle C \rangle) = \frac{n^{nX+1} \mathrm{e}^{-n}}{(nX)!}, \tag{4.22}$$

where $n = 1/C(0,t)$ as defined in § 3 is the number of sheets needed to maintain the average coarse-grained concentration $\langle C \rangle$ constant when $C(0,t)$ decreases. Obviously, $\langle k \rangle = K/N = n$ and

$$\frac{C}{\langle C \rangle} = \frac{k}{n}. \tag{4.23}$$

The maximum entropy distribution of (4.22) is compared in figure 12 with the gamma distribution of (2.2). Both present the same positively skewed shape and are close in absolute values, although $P_E(C)$ decreases faster than in an exponential manner (i.e. like $\exp\{-nX \ln(nX)\}$) at large excursion. Both distributions tend towards the

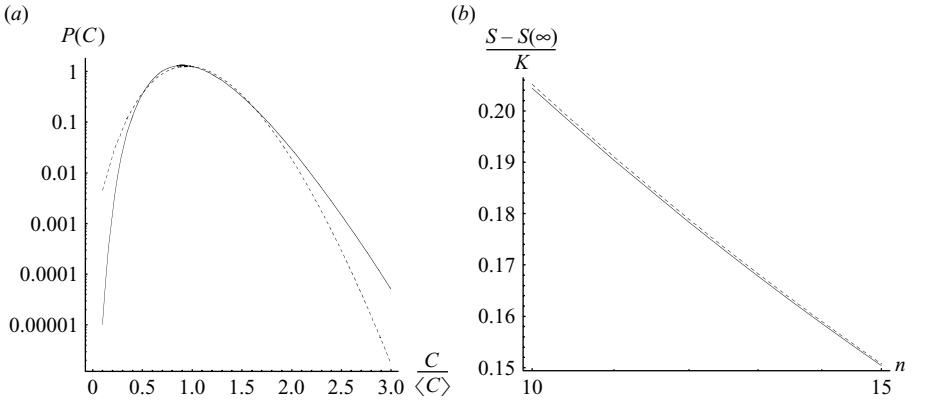

FIGURE 12. (*a*) The maximal entropy concentration distribution (broken line) $P_{\mathrm{E}}(C/\langle C\rangle)$ derived in (4.22) compared to the gamma distribution (continuous line) of (2.2) for $n=10$. (*b*) Corresponding entropies as n is varied.

Gaussian with precision $1/\sqrt{n}$ according to the standard result

$$\frac{1}{\sqrt{2\pi\sigma}}\exp\left(-\frac{(X-1)^2}{2\sigma^2}\right) \quad \text{with} \quad \sigma^2=\frac{1}{n}. \tag{4.24}$$

Defining the entropy of the distribution p_k by $S=\ln w$ (after Gibbs 1901), from the number of states of (4.17) one has

$$\frac{S-S_\infty}{N}=-\sum_{k=0}^{K}\left(p_k\ln p_k+p_k k\ln\frac{k}{\langle k\rangle}\right) \tag{4.25}$$

or

$$\frac{S-S_\infty}{K}=-\frac{1}{\langle k\rangle}\sum_{k=0}^{K}\left(p_k\ln p_k+p_k k\ln\frac{k}{\langle k\rangle}\right), \tag{4.26}$$

where $S_\infty=\langle k\rangle N\ln N=K\ln N$ is the entropy of the uniform distribution with $k=\langle k\rangle$ objects in each of the N coarse-grained cells. The entropy of the uniform distribution S_∞ is proportional to the number of sheets K. As expected, the entropies of the Poisson and gamma distributions are very close and larger than that of the uniform distribution (i.e. $S-S_\infty$ is positive) but by a small amount decreasing logarithmically with $\langle k\rangle=n$, as shown in figure 12.

The random addition of the scalar sheets by a continuous process, which is the aggregation scenario described in § 3 giving rise to the gamma distributions, thus produces a composition field which is slightly different from the sampling of a purely random spatial dispersion of the sheets. In particular, and contrary to the intuition of J. W. Gibbs, the composition field obtained by random stirring is *not* the one with maximal entropy (Gibbs 1901; see in particular the excellent chapter XII in which he devises an analogy for a maximum entropy system based on 'stirring colouring matter' in a fluid). As long as the mixture evolves by self-convolution, it does not reach 'thermal equilibrium'. Celani & Seminara (2005), using different arguments, arrive at the same conclusion. However, both processes lead to uniformity along nearby paths.

5. Scalar dissipation

5.1. *Dissipation*

The shape of the overall concentration distribution $P(C)$ and its rate of evolution in time give access to the scalar dissipation rate (Zeldovich 1937)

$$\chi = -\frac{\mathrm{d}}{\mathrm{d}t}\langle C^2\rangle = 2D\langle(\nabla C)^2\rangle, \tag{5.1}$$

a quantity of fundamental interest and sometimes modelled for closure purposes. Starting with the Laplace transform of the distribution of the confined mixture for which the average concentration is conserved $\tilde{P}(s) = (1 + (s/n)\langle C\rangle)^{-n}$, one has

$$\langle C^2\rangle = \langle C\rangle^2 \left.\frac{\partial^2}{\partial s^2}\tilde{P}(s)\right|_{s=0}, \tag{5.2}$$

that is

$$\frac{\langle C^2\rangle}{\langle C\rangle^2} = 1 + \frac{1}{n}, \tag{5.3}$$

with $n = 1/C(0,t) \sim (t/t_s)^{5/2}$, the order of the corresponding gamma distribution. Therefore, for *finite* t_s, that is for $D \neq 0$ and for $t > t_s$,

$$\chi = \frac{\langle C\rangle^2}{t_s}\left(\frac{t}{t_s}\right)^{-7/2}. \tag{5.4}$$

The dissipation χ shifts towards zero as $t/t_s \to \infty$. When $D \to 0$, that is for $t_s \to \infty$, χ remains equal to zero at all times. For these kinds of flows at least, there is obviously no way to alter the concentration distribution of a mixture in the limit of a vanishingly small scalar diffusivity. Balmforth & Young (2003) provide a similar discussion in the context of heat transfer at a wall: the injection of scalar fluctuations is diffusion-limited at the wall, so that χ goes to *zero* in the stirred bulk as the scalar diffusivity vanishes (see also Falkovich, Gawedzki & Vergassola 2001 on the distinguished limits $t \to \infty$ versus $D \to 0$ and the so-called dissipation anomaly).

Note finally that the spatial scale δ associated with the decay of χ is the width of the scalar gradient, given by $\sqrt{Dt}$ at large times, and not the coarse-grained scale η. Indeed, χ defined in (5.1) can be written as

$$\chi \sim Dn(t)\frac{C(0,t)^2}{\delta^2}, \tag{5.5}$$

where the gradient squared $(\nabla C)^2$ is written as $(C(0,t)/\delta)^2$ with $C(0,t) \sim (t/t_s)^{-5/2}$, the maximal concentration of a sheet. With the number of sheets $n(t) \sim (t/t_s)^{5/2}$, owing to the temporal decay of χ from (5.4) it is found that

$$\delta \sim \sqrt{Dt} \tag{5.6}$$

consistently with the scaling of the diffusion profile transverse width of a single isolated sheet after the mixing time (see Appendix A).

5.2. *Conditional dissipation*

The typical width of the gradient $\delta \sim \sqrt{Dt}$ becomes, for the mixture confined in the channel, of the order of the resolution scale of the images, allowing a direct computation of $\langle D(\nabla \boldsymbol{C})^2\rangle$. A further indication that the dissipation scale is effectively resolved is that the two ways of computing the dissipation rate from the recorded fields $\mathrm{d}\langle C^2\rangle/\mathrm{d}t$ and $2D\langle\nabla\, C^2\rangle$ match.

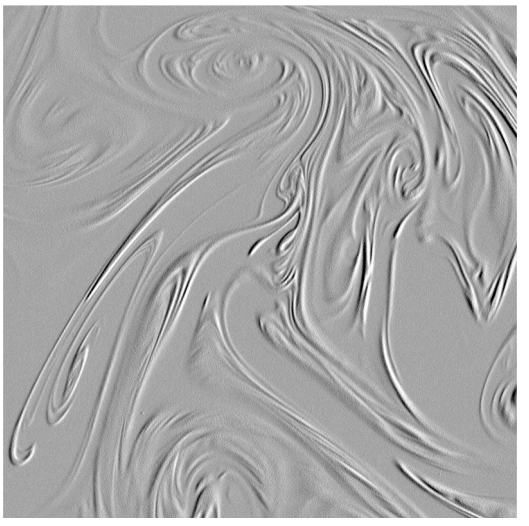

FIGURE 13. Transverse concentration gradient in the confined mixture experiment at $t/t_s \approx 3$ for $Sc = 2000$.

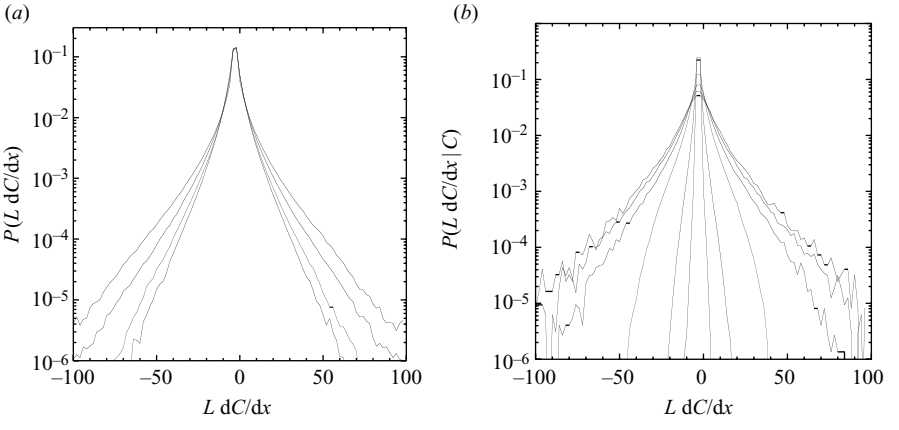

FIGURE 14. (*a*) Transverse gradient distribution at $t/t_s = 1, 1.5, 2, 3$. (*b*) Conditional transverse gradient distribution, for $C/\langle C\rangle = 1/4, 1/2, 1, 2, 3, 4$ and $t/t_s = 1$. The variance of the gradient distribution increases with C. $Sc = 2000$.

The analysis of the gradient distribution shows that the mixture is nearly isotropic (figure 13), as the amplitudes of transverse (y direction) and longitudinal (x direction) gradients are nearly equal ($\langle|\partial_y C|\rangle = 0.9\langle|\partial_x C|\rangle$). By symmetry, we further assume that, when computing the total dissipation, the statistics of $\partial_z C$, the component of the gradient normal to the observation plane, are identical to those of the component measured in the plane $\partial_y C$, on average. The total gradient distribution presents symmetrical exponential tails (figure 14), which are associated with large deviations of the concentration C as can be seen on the conditional gradient distribution. The conditional dissipation $\langle D(\nabla C)^2|C\rangle$ is thus an increasing function of the concentration (figure 15). The latter quantity is often measured in numerical simulations or modelled as a closure term for the evolution of concentration distribution, since it permits one to infer $P(C, \boldsymbol{x}, t)$ by the Liouville transport equation when the scalar is transported by a velocity field $\boldsymbol{u}(\boldsymbol{x}, t)$ (see e.g. Pope 1985; Sinai & Yakhot 1989; Dopazo 1994;

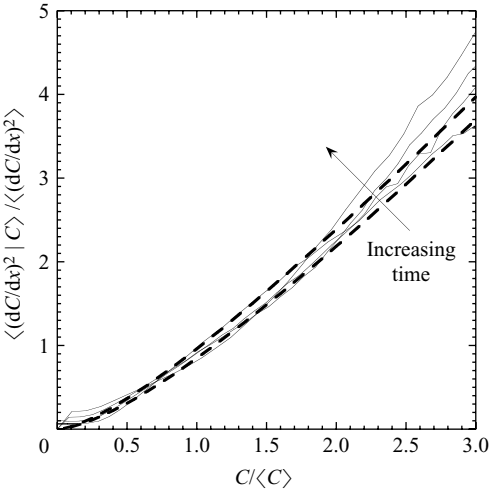

FIGURE 15. Conditional dissipation for t/t_s, varying from 1 to 3 at $Sc = 2000$. Dashed lines correspond to (5.10) for $n = 1$ and $n = 4$, the corresponding orders of the concentration distribution at time $t/t_s = 1$ and $t/t_s = 3$. For larger values of n, the curves superimpose with that obtained for $n = 4$. The probability that $C/\langle C\rangle$ exceeds 2 for gamma distributions of the order $n > 5$ is smaller than 0.03; consequently the slight mismatch between experimental data and the prediction is immaterial.

Fox 2004; Sawford 2004). It obeys

$$[\partial_t + \nabla\cdot\langle \boldsymbol{u} \mid C\rangle]P(C, \boldsymbol{x}, t) = -\partial_C[\langle D\nabla^2 C \mid C\rangle P(C, \boldsymbol{x}, t)] \tag{5.7}$$

or alternatively, using $\nabla^2 P = -\partial_C[(\nabla^2 C \mid C)P] + \partial_{C^2}[((\nabla C)^2 \mid C)P]$ (see Dopazo 1979; Pope 2000),

$$[\partial_t + \nabla\cdot\langle \boldsymbol{u} \mid C\rangle]P(C, \boldsymbol{x}, t) = D\nabla^2 P(C, \boldsymbol{x}, t) - \partial_C^2[\langle D(\nabla C)^2 \mid C\rangle P(C, \boldsymbol{x}, t)]. \tag{5.8}$$

Since the confined mixture is statistically homogeneous in the direction transverse to the flow, this becomes

$$\partial_t P + \partial_x[\langle u_x \mid C\rangle P] = D\partial_x^2 P - \partial_C^2[\langle D(\nabla C)^2 \mid C\rangle P]. \tag{5.9}$$

The conditional dissipation $\langle D(\nabla C)^2 \mid C\rangle$ can then be deduced from the shape and temporal dependence if it is assumed that the correlation between velocity and concentration is weak (i.e. $\partial_x\langle u_x \mid C\rangle \simeq 0$) and the diffusive term negligible, assumptions whose consistency will be checked *a posteriori*.

With concentration distributions gamma distributed (i.e. $P(C/\langle C\rangle) \equiv \Gamma_n(C/\langle C\rangle)$) of order $n(t)$, one gets, integrating $\Gamma_n(C/\langle C\rangle)$ twice with respect to C and differentiating it with respect to $n(t)$,

$$\begin{aligned}
&D\langle (\nabla C)^2 \mid C\rangle \frac{(n\,X)^n\,\Gamma(n)}{\langle C\rangle^2}\Gamma_n(X)\\
&\quad = -\frac{\mathrm{d}n}{\mathrm{d}t}[n^{-2+n}\,X^n\,(\Gamma(1+n, n\,X) + n^2\,X\,\Gamma(n, n\,X)\,\log(n)\\
&\qquad - n\,\Gamma(1+n, n\,X)\,\log(n) + n^2\,X\,\Gamma(n, n\,X)\,\log(X)\\
&\qquad - n\,\Gamma(1+n, n\,X)\,\log(X) + n^2\,x\,\mathrm{MeijerG}(\{\{\}, \{1, 1\}\}, \{\{0, 0, n\}, \{\}\}, n\,X)\\
&\qquad - n\,\mathrm{MeijerG}(\{\{\}, \{1, 1\}\}, \{\{0, 0, 1+n\}, \{\}\}, n\,X)\\
&\qquad - n^2\,X\Gamma(n, n\,X)\,\mathrm{PolyGamma}(0, n) + n\,\Gamma(1+n, n\,X)\,\mathrm{PolyGamma}(0, n))],
\end{aligned} \tag{5.10}$$

where $X = C/\langle C\rangle$. PolyGamma$(0, n) = (\mathrm{d}\Gamma(n)/\mathrm{d}n)/\Gamma(n)$ and MeijerG denotes the Meijeir's G-function, written here in the Mathematica$^{\mathrm{TM}}$ syntax. This complicated formula is very well fitted with

$$\frac{D\langle(\nabla C)^2 \mid C\rangle}{\chi} \simeq 0.96\left(\frac{C}{\langle C\rangle}\right)^{1.4} \tag{5.11}$$

for $0 < C/\langle C\rangle \lesssim 3$. The fair agreement between the experimental measurement of the conditional scalar dissipation and the prediction in (5.10) derived from the self-convolution construction of $P(C, t)$ is an *a posteriori* proof that $\partial_x\langle u_x \mid C\rangle \simeq 0$ in the present flow or at least that the value of this correlation as well as the magnitude of the diffusive term $D\partial_x^2 P$ have no appreciable consequence on the evolution equation linking the concentration distribution with the conditional dissipation. The conditional dissipation is an increasing function of the concentration level. This is consistent with observations in Jayesh & Warhaft (1992), where temperature fluctuations are injected in an air stream by the means of thin heated wires (the 'mandoline'), thus realizing an initially segregated concentration field like the one in the present experiments. In the same conditions, the concentration distribution is positively skewed. The same authors also report a U shape, symmetrical about the mean conditional dissipation in the presence of a mean large-scale concentration gradient giving rise to a *symmetrical concentration distribution*. Direct numerical simulation (DNS) data are usually obtained for symmetrical situations in which the hot (coloured) fluid parcels are evenly spread among cold (clear) parcels (see Eswaran & Pope 1988; Fox & Raman 2004; see also Fox 1994 for a counter example). In that case, both the concentration pair distribution function (PDF) and the conditional dissipation are symmetric, by construction. Our experiments, in which $\langle C\rangle$ is always smaller than 1/2, retain an imprint of their original asymmetry for the whole mixture evolution, as concentration fluctuations arise positively from essentially zero, the diluting medium concentration baseline: this is the *elementary sheet* description of the scalar field. The higher concentration levels are associated with the steepest concentration gradients, whereas the lowest concentrations are associated with smoother gradients, hence the shape of the conditional dissipation $\langle D(\nabla C)^2 \mid C\rangle$ dependence on C shown in figure 15.

The singular case of symmetrical mixtures (i.e. with a symmetrical concentration distribution) is to be discussed along the same lines except that concentrations are counted from the mean rather from zero (see Appendix B).

5.3. *Mapping closure approximation*

The probability density function of some concentration field C may be represented through a mapping function $X(\psi, \boldsymbol{r}, t)$, such that $C(\boldsymbol{r}, t) = X(\psi(\boldsymbol{r}, t), \boldsymbol{r}, t)$, with ψ a Gaussian variable. For simplicity, the mapping can be chosen so that the variance of the ψ distribution is equal to 1 for every spatial location $\boldsymbol{r}$ and all values of time t. Since we are considering homogeneous concentration fields, the mapping function X does not in fact depend on $\boldsymbol{r}$, and it can be deduced from the equality

$$\mathscr{P}(X(\psi, t), t) = \mathrm{erf}(\psi/\sqrt{2}), \tag{5.12}$$

where $\mathscr{P}(C, t) = \int_0^C P(c, t)\,\mathrm{d}c$ denotes the cumulative distribution of $P(C, t)$. This defines the unique mapping $C = X(\psi)$ that is an increasing function of ψ.

For a homogeneous flow, the evolution equation for the concentration distribution is, as already noted,

$$\frac{\partial P(C,t)}{\partial t} = -\frac{\partial D\langle \Delta C \mid C\rangle P}{\partial C}. \tag{5.13}$$

Consequently, $\mathrm{d}_t\mathscr{P}(X(\psi,t),t) = \partial_t X(\psi,t)P(X,t) - D\langle \Delta C \mid \psi\rangle P(X,t) = 0$, and thus

$$\frac{\partial X(\psi,t)}{\partial t} = D\langle \Delta C \mid \psi\rangle = D\left(\left(\frac{\partial X}{\partial \psi}\right)\langle \Delta\psi \mid \psi\rangle + \left(\frac{\partial^2 X}{\partial \psi^2}\right)\langle (\nabla\psi)^2 \mid \psi\rangle\right). \tag{5.14}$$

This representation has been found convenient, since in the longtime limit, as the concentration distribution tends towards the Gaussian, the mapping function tends towards a linear relationship between ψ and C. There can be an interpretation of (5.14) as a convection diffusion equation of X in the ψ space, leading to a linearization of the profile $X(\psi)$ at large time.

The mapping closure approximation developed by Chen, Chen & Kraichnan (1989) and Kimura & Kraichnan (1993) allows to make a prediction of the evolution equation of X through a supplementary assumption on the ψ field: it is assumed that ψ is a multivariate Gaussian field, which implies that the two-point distribution $P(\psi(\boldsymbol{r}_1), \psi(\boldsymbol{r}_2))$ is also Gaussian. This has consequences on the statistics of the derivative of ψ, since under this assumption $\langle (\nabla\psi)^2 \mid \psi\rangle = \langle (\nabla\psi)^2\rangle$ is independent of ψ, and $\langle \Delta\psi \mid \psi\rangle = -\psi\langle (\nabla\psi)^2\rangle/\langle\psi^2\rangle$, where $\langle\psi^2\rangle = 1$ has been used. Then, (5.14) becomes

$$\frac{\partial X}{\partial t} = D\langle \nabla\psi^2\rangle\left(-\psi\frac{\partial X}{\partial \psi} + \frac{\partial^2 X}{\partial \psi^2}\right). \tag{5.15}$$

There are thus two contributions to the evolution of X versus ψ: First, $\partial_t X = -D\langle \nabla\psi^2\rangle\psi\partial_\psi X$ is a dilatation around $\psi = 0$ of the X shape. This is related to the decrease of the variance of the concentration distribution, without any change in the distribution shape. Second, $\partial_t X = -D\langle \nabla\psi^2\rangle\partial_\psi^2 X$ is a diffusion process of the X shape, making it tend towards a linear function of ψ, corresponding to a concentration distribution tending towards the Gaussian. However, the assumption that ψ is a multivariate Gaussian field has no fundamental reason to be fulfilled for real concentration fields and is not in general: this assumption implies in particular that the distribution of $\nabla\psi$ for a given value of ψ is Gaussian, which also implies that the distribution of $\nabla C = \partial_\psi X\nabla\psi$ for the value $C = X(\psi)$ is Gaussian, a fact that is notably not true (see e.g. figure 14). We now make an attempt at proposing corrections for (5.15).

The self-convolution process that is described in § 3 also leads to a reduction of the concentration variance and an evolution of the distribution shape: the concentration distribution is found to be a gamma distribution of order $n(t)$, with variance $1/n$. The corresponding mapping function X can be computed (figure 16), and its evolution can be compared with (5.15). The major effect is the variance reduction, so that it is useful to use a new set of rescaled variable

$$\left.\begin{aligned} n = n(t) &= \langle C\rangle^2/\sigma_C^2, \\ \underline{\psi} &= \psi\sigma_C/\langle C\rangle = \psi/n^{1/2}, \end{aligned}\right\} \tag{5.16}$$

where σ_C^2 denotes the scalar variance. Using these variables, (5.15) is written as

$$\frac{\partial X}{\partial n} = \frac{1}{2n^2}\frac{\partial^2 X}{\partial \underline{\psi}^2}, \tag{5.17}$$

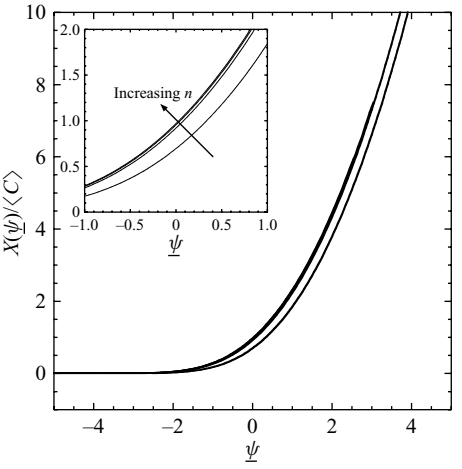

FIGURE 16. Mapping function for gamma distribution of the order $= 1, 4, 7, 10$.

while the whole of (5.14) becomes

$$\frac{\partial X}{\partial n} = \left(\frac{1}{2n^2}\right)\left(\left(\frac{\partial X}{\partial \underline{\psi}}\right)\left[n\underline{\psi} + \langle \Delta \underline{\psi} \mid \underline{\psi}\rangle \frac{\langle C\rangle^2}{\langle (\nabla C)^2\rangle}\right] + \left(\frac{\partial^2 X}{\partial \underline{\psi}^2}\right)\left[\langle (\nabla \underline{\psi})^2 \mid \underline{\psi}\rangle \frac{\langle C\rangle^2}{\langle (\nabla C)^2\rangle}\right]\right). \tag{5.18}$$

This evolution equation can be approached by a general form

$$\frac{\partial X}{\partial n} = \left(\frac{1}{2n^2}\right)\left(\left(\frac{\partial X}{\partial \underline{\psi}}\right)\mathscr{U} + \left(\frac{\partial^2 X}{\partial \underline{\psi}^2}\right)\mathscr{D}\right), \tag{5.19}$$

where $\mathscr{U}$ and $\mathscr{D}$ are constant. (For the mapping closure approximation $\mathscr{U} = 0$ and $\mathscr{D} = 1$.) Choosing $\mathscr{U} \approx 0.3$ and $\mathscr{D} \approx 0.6$ nearly equilibrates both sides of (5.19), with a mismatch smaller than 10%. Of course the new evolution equation obtained for the mapping evolution is incomplete, as it does not conserve the average concentration, but this is at least a good approximation in the central region $\underline{\psi} \in [-2\ 2]$. The corresponding values are compared with the experimental measurement of $[n\underline{\psi} + \langle \Delta \underline{\psi} \mid \underline{\psi}\rangle(\langle C\rangle^2/\langle (\nabla C)^2\rangle)]$ and of $[\langle (\nabla \underline{\psi})^2 \mid \underline{\psi}\rangle(\langle C\rangle^2/\langle (\nabla C)^2\rangle)]$ in figure 17. A significant disagreement is found between experimental data and both the mapping closure approximation and the gamma distribution sets. However, it is through an arbitrary choice that $\mathscr{U}$ and $\mathscr{D}$ are independent of $\underline{\psi}$ for the gamma distribution set, and since in (5.19) both $\partial_{\underline{\psi}} X$ and $\partial^2_{\underline{\psi}} X$ are positive, an overestimation of $\mathscr{U}$ leads to an underestimation of $\mathscr{D}$.

Hence the mapping evolution equation cannot be written as simply as (5.19), with constant coefficients, and the dependence of $\mathscr{U}$ and $\mathscr{D}$ on $\underline{\psi}$ has to be taken into account. These forms cannot be uniquely determined from the gamma distributions evolution together with (5.19) either; this failure is a consequence of the fundamental premise of the Mapping Closure Approximation: the two-point statistics of the scalar field is not Gaussian (see e.g. figure 14). Spatial correlations, reflected by the existence of a coarsened scale much larger than the dissipation scale (§ 4.1), unavoidably dismiss this assumption.

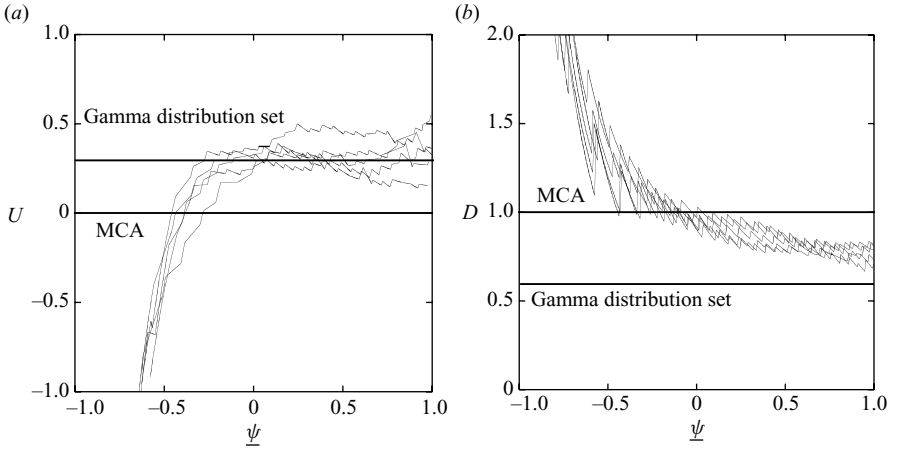

FIGURE 17. (*a*) Experimental measurement of $[n\underline{\psi} + \langle \Delta\underline{\psi} \mid \underline{\psi}\rangle\langle C\rangle^2/\langle(\nabla C)^2\rangle]$ for $1 \leqslant n \leqslant 3$ and comparison with prediction of the mapping closure approximation (MCA) and the gamma distributions set evolution (with $\mathscr{U}$ taken to be constant). (*b*) Experimental measurement of $[\langle(\nabla\underline{\psi})^2 \mid \underline{\psi}\rangle\langle C\rangle^2/\langle(\nabla C)^2\rangle]$ for $1 \leqslant n \leqslant 3$ and comparison with prediction of the mapping closure approximation and the gamma distribution set evolution (with $\mathscr{D}$ taken to be constant).

6. Conclusion and further remarks

We have analysed mixtures evolving under confinement. In this limit, the particles are forced to aggregate, that is to add to their concentration levels. As soon as the mixture is stirred in a more or less random manner, the addition is made *at random* among the levels available in the current distribution. This operation implies that the concentration distribution evolves by self-convolution and, when it does, gives an *a posteriori* precise definition of what 'random' means. The kinetic equation expressing this process (3.14) gives rise to stable gamma distributions. They have been found to represent accurately the content of a mixture keeping its average concentration $\langle C\rangle$ constant, as well as its rate of deformation in time (§§ 2 and 3).

We would like to close with some remarks on the consistency and limits of, and the questions opened on, the aggregation scenario we have presented here:

(i) The addition of random variables erases the differences from the mean as a general property of the central limit theorem (Feller 1970), and it is generally agreed that this process is the recipe for making Gaussian distributions. This is indeed true at the limit of a very large number of composition operations and when one is interested in the shape of the distribution around its maximum, at the precision of its standard deviation (see e.g. the discussion in § 4.2). It is clear that the bell-shaped concentration distributions close to the uniform limit in the channel flow (see figure 6) might well be approximated by Gaussians. However, we have shown how the mixture evolution selects a particular route towards uniformity, directed by an aggregation process, which pertains to the central limit paradigm, as it involves sums of random variables, but which does not imply, in its transient development, Gaussians.

(ii) The aggregation scenario ignores the fluctuations in the elongation rate, which are large in turbulent flows (Voth, Haller & Gollub 2002). These are revealed by the shape of the 'bare' distribution of an ever-dispersing mixture, such as the one shown in figures 19 and 20, for which $P(C)$ never converges with a gamma distribution (Villermaux, Innocenti & Duplat 1998; Villermaux & Innocenti 1999; Villermaux, Innocenti & Duplat 2001; Lavertu & Mydlarski 2005). Conversely, the aggregation

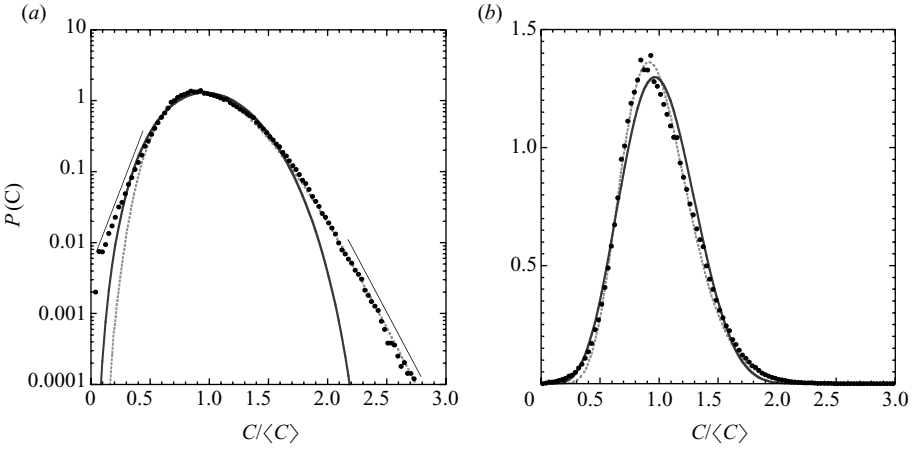

FIGURE 18. A comparison between real data obtained in the channel flow at $(x-d)/L=1.5$ and $Re=2\times10^3$ with $\langle C\rangle=0.4$ (●), the gamma distribution with $n=11.5$ (dotted line) and the beta distribution with same mean and variance (continuous line). (*a*) In log–lin scales. (*b*) In lin–lin scales. The fit by the beta distribution may look satisfactory in lin–lin scales (although the distribution is not well described around its maximum), but its inadequacy is evident in log–lin scales: the beta distribution does not capture the exponential fall-off, originating from the aggregation process at the core of the distribution construction, unlike the gamma distribution. The figure also shows the limits of the diluted limit giving rise to gamma distributions. The low concentration side of the distribution departs from the pure gamma shape for an average concentration close to 1/2.

FIGURE 19. A snapshot of a dispersing plume made by the injection of a dye through a small tube of diameter $d=8$ mm on the axis of a larger turbulent jet whose integral scale is $L=8$ cm at the injection location. $Re=u'L/\nu=10^4$.

scenario does not hold for such a mixture, which disperses so fast that sheets have no time to merge. However, these fluctuations of concentration due to unequal elongations among different sheets which have not interacted at a given instant of time are progressively hindered by the aggregation process, when it has a chance to occur, as for the confined mixture.

A natural question to ask is whether, for any given flow, aggregation takes over dispersion. The more dispersing the mixture, the less chance sheets have to meet and aggregate. A simple estimate is to compare the rate of decrease of the average

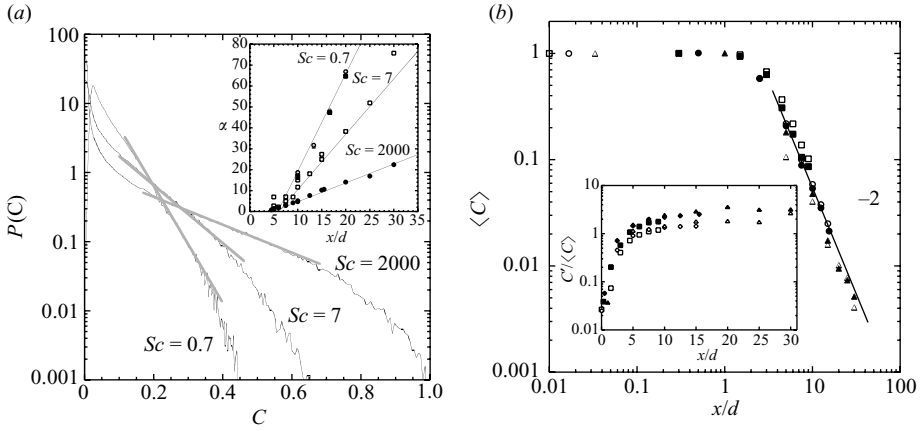

FIGURE 20. (*a*) Concentration distributions $P(C)$ of the ever-dispersing mixture of figure 19 recorded at $x/d = 10$ for three different Schmidt numbers. The shape of the distributions is exponential near the grey-shaded regions like $P(C) \sim \exp(-\alpha C)$. Insert: The argument α for different downstream locations x/d, Reynolds numbers and three Schmidt numbers. ●: $Sc = 2000$, $Re = 6000$ and 12 000, $d/L = 0.05, 0.1, 0.6$. □: $Sc = 7$, $Re = 6000$, $d/L = 0.05, 0.1, 0.16$. ■: $Sc = 0.7$, $d/L = 0.08$, $Re = 23\,000$. ○, △: $Sc = 0.7$, $d/L = 0.08$, $Re = 45\,000$. (*b*) Downstream evolution of the average concentration $\langle C \rangle$ in the ever-dispersing mixture of figure 19 for three different injection diameters and two Schmidt numbers. Insert: Downstream evolution of the fluctuations $C'/\langle C \rangle = \sqrt{\langle C^2 \rangle / \langle C \rangle^2 - 1}$. $Re = 6000$, $d/L = 0.05$ (▲), 0.1 (■), 0.16 (●), $Sc = 2000$. For $Sc = 7$, same open symbols.

concentration $(-\mathrm{d}\langle C \rangle/\mathrm{d}t)/\langle C \rangle$, representative of the dispersive properties of the mixture, with the mixing time t_s^{-1}. As long as $(-\mathrm{d}\langle C \rangle/\mathrm{d}t)/\langle C \rangle > t_s^{-1}$, the mixture disperses so fast that particle interaction is unlikely. Estimating $(-\mathrm{d}\langle C \rangle/\mathrm{d}t)/\langle C \rangle \sim u/d$ for the dispersing mixture in figure 19 and $t_s \sim (d/u)Sc^{1/5}$, aggregation is not likely to occur once $Sc > 1$. The case $Sc = 0.7$ is borderline, and indeed the cusp of $P(C)$ at $C = 0$ is less pronounced than for $Sc = 7$ and $Sc = 2000$, as seen in figure 20, indicating some amount of self-convolution. When $\langle C \rangle$ is conserved through time, however, aggregation takes over, at a rate prescribed by the average mixing time.

(iii) An interesting consequence of the aggregative vision is the existence of a very large scale in the scalar field compared to the usual scales resulting from local balances (§ 4.1). That length scale $\eta = LSc^{-2/5}$ is the transverse size of the domains in the flow in which the concentration C is defined. It results from the coalescence of bundles of sheets under the action of a large-scale strain, established at the integral scale of the flow L. As opposed to local balances setting the size of the fine-scale gradient of the elementary sheets, this new scale results from a non-local fusion mechanism consistent with the construction mechanism of the concentration distribution.

(iv) The beta distribution

$$P(C) = \Gamma(a+b)/\Gamma(a)\Gamma(b)C^{a-1}(1-C)^{b-1} \tag{6.1}$$

with a and b the functions of the concentration mean and variance is often used as a convenient fit for the concentration distribution in modelling (Fox 2004). Besides the fact that it has no chance to 'look like' a gamma distribution on a log scale (and it does not indeed; see figure 18), in particular because it does not fall exponentially, the beta distribution does not present the decisive property of being stable by self-convolution, a property which, as this study suggests, is mandatory for confined mixtures.

(v) We have purposely formalized the aggregation scenario and the corresponding kinetic equations in the *diluted limit*: concentration levels C are counted from 0 to 1, and we add random variables from 0. This obviously applies to situations in which elementary sheets are well defined in a zero-concentration environment. In other words, this limit applies well for mixtures in which the white mixes in the black with an average concentration of white $\langle C\rangle$ below 1/2. Otherwise, the concentration C would represent that of the black in the white, and the distribution would be skewed the other way. This does not cause any principle problem, since diffusion is a linear phenomenon, and C can well be defined as $1-C$. However, for mixtures incorporating as much white as black, the mean field description we have adopted would rather suggest counting concentration levels from $\langle C\rangle$, that is defining $c=C-\langle C\rangle$ and deriving the same convolution equations for $p(c)$. Fourier (because c can now be negative) rather than Laplace transforms of the corresponding kinetic equations indicate that now the distributions have exponential tails on both sides of the mean, the negative wing representing black sheets aggregating in a grey medium at the average concentration (see figure 18 and Appendix B).

(vi) The success of the random aggregation scenario, and the associated self-convolution construction of $P(C)$, is in itself an enigma. We have adopted this rule because of the clue experimental facts presented here, but this rule is, in our analytic treatment, an *ad hoc* assumption. It works so well that it is very likely to have a deep fundamental origin. In particular, the key point to address would be to understand why the 'maximal randomness hypothesis' expressed by the convolution operation, disregarding correlations in the medium in the composition operation, works so well. This question could be investigated by perhaps using simple stirring protocols as the deterministic maps familiar in ergodic theory (Arnold & Avez (1967), coupled with diffusive smearing. These approaches have already succeeded to recover mixing times in some cases (Fannjiang, Nonnenmacher & Wolonski 2004) and may succeed in deriving the self-convolution property of $P(C)$ from first principles – and appropriate maps.

We are indebted to Claudia Innocenti, with whom this study started, and to Jean-Paul Barbier Neyret for his decisive help with data acquisition. Over the years, this work has been supported by the Sociéte Europénne de Propulsion (SEP) under contract 910023, the Centre National d'Études Spatiales (CNES) under contract 02-0485-00 and the Centre National de la Recherche Scientifique (CNRS) and the Agence Nationale de la Recherche (ANR) through grant ANR-05-BLAN-0222-01.

Appendix A. Stretching enhanced diffusion

Focus on the scale of the elementary scalar sheets visible from the intercept with the visualization plane (figure 19). It is known that a succession of random stretching motions applied to passive objects form sheets (Betchov 1956; Girimaji & Pope 1990; Duplat & Villermaux 2000) for which there is some experimental evidence (see Ottino 1989; Buch & Dahm 1996). Let us consider a *single* sheet, and let C be the scalar concentration in the vicinity of the sheet and z a coordinate in the direction normal to the iso-concentration surface C. The diffusive uniformization of the dye is enhanced by the stretching of the underlying motions. The convection–diffusion transport equation for C reduces (see e.g. Levque 1928; Mohr, Saxton & Jepson 1957; Marble & Broadwell 1977; Ranz 1979; Rhines & Young 1983; Allgre & Turcotte 1986; Marble 1988; Ottino 1989; Beigie, Leonard & Wiggins 1991; Meunier & Villermaux 2003; Fannjiang *et al.* 2004) to a one-dimensional problem when the radius

of curvature of the iso-concentration surface is large compared to the lamella thickness (Dimotakis & Catrakis 1999). Let $s(t)$ be the distance between two material particles in the direction z perpendicular to a sheet and

$$\gamma(t) = \frac{\mathrm{d}\ln\{s(t)\}}{\mathrm{d}t} \tag{A 1}$$

its rate of compression. The mass conservation equation of a species with diffusion coefficient D then becomes

$$\frac{\partial C}{\partial t} + \gamma(t) z \frac{\partial C}{\partial z} = D\frac{\partial^2 C}{\partial z^2}. \tag{A 2}$$

By the change of variables

$$\tau = D\int_0^t \frac{\mathrm{d}t'}{s(t')^2} \quad \text{and} \quad \xi = \frac{z}{s(t)}, \tag{A 3}$$

(A 2) is reduced to a simple diffusion equation

$$\frac{\partial C}{\partial \tau} = \frac{\partial^2 C}{\partial \xi^2}. \tag{A 4}$$

Suppose that the lamella has an initial width s_0 and uniform concentration, so that its concentration profile is 'top hat'. At any later time, its concentration profile is the solution of (A 3) (see e.g. Villermaux & Rehab 2000; Meunier & Villermaux 2003) from which it follows that the maximal concentration in the lamella is

$$C(0, t) = \mathrm{erf}\left(\frac{1}{4\sqrt{\tau}}\right). \tag{A 5}$$

With

$$s(t) = \frac{s_0}{(1+\sigma t)^2}, \tag{A 6}$$

as implied, using mass conservation $\ell(t)^2 s(t) \sim s_0^3$, by the experimentally observed linear increase of material contours lengths and from (A 3),

$$\tau = \frac{1}{5\,Pe}(-1 + (1+\sigma t)^5) \quad \text{with} \quad Pe = \frac{\sigma s_0^2}{D}. \tag{A 7}$$

The mixing time t_s, reached when $\tau = O(1)$, is thus, when the Péclet number Pe is larger than unity,

$$t_s \sim \frac{1}{\sigma} Pe^{1/5} \quad \text{and} \quad C(0, t) \sim \left(\frac{t}{t_s}\right)^{-5/2} \quad \text{for} \quad t > t_s. \tag{A 8}$$

In figure 21 are plotted $s(t)$, the sheet thickness σ_C defined from the variance of the concentration profile

$$\sigma_C^2 = \frac{\displaystyle\int_{-\infty}^{\infty} z^2 C(z, t)}{\displaystyle\int_{-\infty}^{\infty} C(z, t)} \tag{A 9}$$

and the maximal concentration $C(0, t)$ in the course of time (see also Villermaux & Rehab 2000). It is seen that the thickness of the diffusion profile follows the decrease imposed by the kinematics of the flow up to the mixing time. At that moment, the lamella has reduced to a sheet which is aligned parallel to the streamlines of the

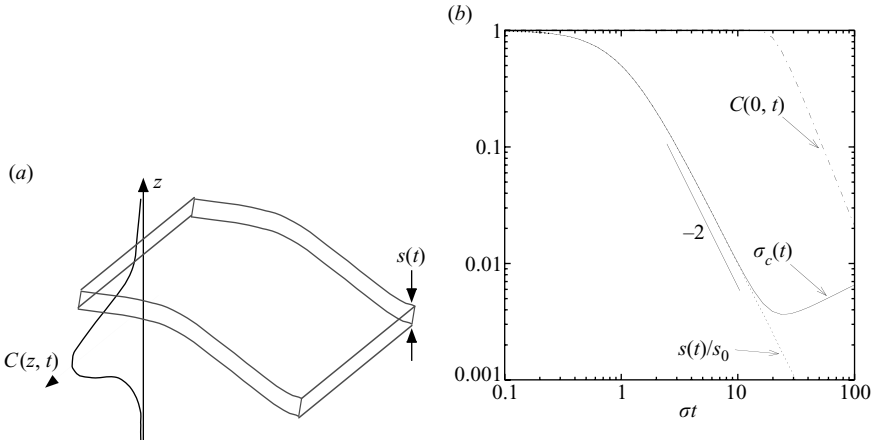

FIGURE 21. (*a*) Sketch of an isolated stretched scalar lamella being compressed in its transverse direction and the associated concentration profile. (*b*) Evolutions as a function of σt and for $Pe = \sigma s_0^2/D = 10^7$ of thickness $s(t)/s_0$ given by (A 6) (dotted line); standard deviation σ_C of the concentration profile across the lamella given by (A 9) normalized by s_0 (continuous line); maximal concentration $C(0, t)$ at the centre of the sheet given by (A 5) (broken line).

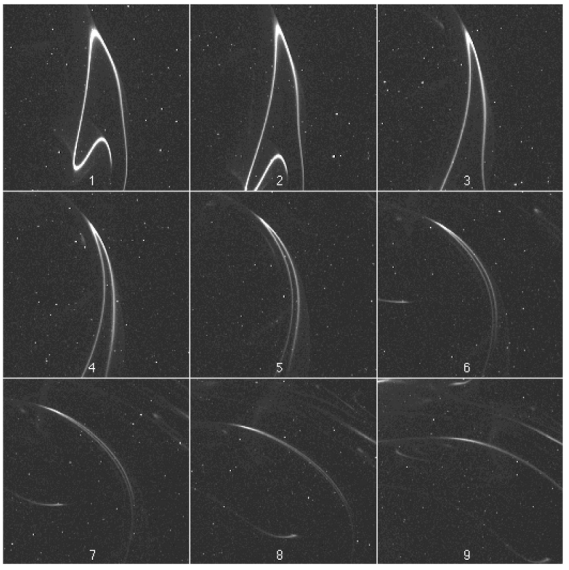

FIGURE 22. A folded sheet seen at consecutive instants of time, embedded in a three-dimensional turbulent flow and undergoing coalescence. The sheet is made visual by a planar two-dimensional cut through the medium. Length and time scales are given in figure 23.

flow after which, for $t \gg t_s$, the maximal concentration $C(0, t)$ decays as $(\sigma t)^{-5/2}$, and the sheet thickness re-increases diffusively like $(Dt)^{1/2}$. (The rate of compression $\mathrm{d} \ln s(t)/\mathrm{d}t$ decays like $1/t$ so that molecular diffusion becomes finally dominant.)

Figure 22 shows how two pieces of a folded sheet embedded at a saddle point of the underlying displacement field are brought close to each other in the dispersing mixture. The distance between the two elements decays like t^{-2}, while the maximal concentration in the sheets decays as $t^{-5/2}$ according to (A 6) and (A 8), as seen in figure 23. The concentration field resulting from the interpenetration of the two sheets

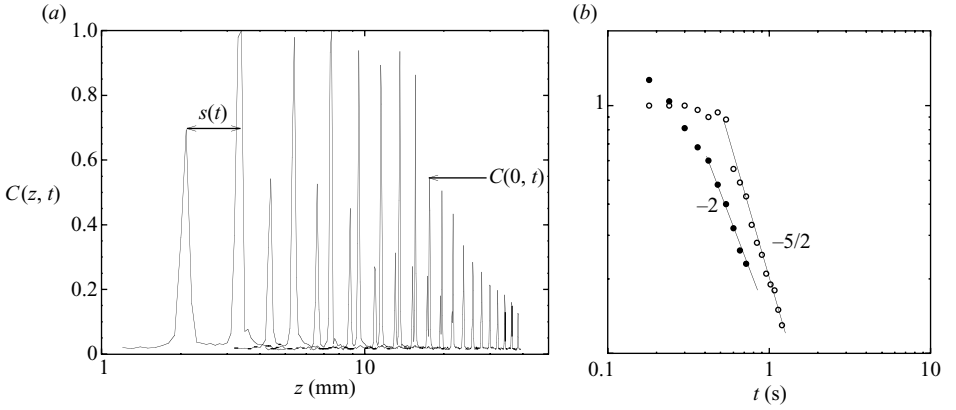

FIGURE 23. (*a*) Spatial concentration profiles $C(z,t)$ of the folded coalescing sheet shown in figure 22, superimposed for successive instants of time. The sheet moves perpendicular to itself, as its two pieces get closer; the figure shows the concentration profiles resulting from the intersection of the sheet in figure 22 with a line fixed in space. (*b*) The distance $s(t)$ between the maxima of concentration of the profiles (●) and the evolution of the maximal concentration $C(0,t)$ of the overall profile (○) as a function of time.

is the *addition* of the concentration profiles of each individual sheet, a consequence of the linearity of the Fourier diffusion equation (Fourier 1822).

Appendix B. Convolutions around the mean

We derive here the shape of the concentration distribution evolving through the self-convolution process described in § 3, counting now the concentration levels not from 0 but from the average concentration $\langle C\rangle$. We therefore define a concentration c such that $c = C - \langle C\rangle$, and we look for its distribution $p(c)$. For the same reason which is outlined in § 3 – and which basically comes from the linearity of the Fourier diffusion equations – the concentration levels c obey an addition rule, whose translation in the probability space of $p(c)$ is a self-convolution process. The concentration c can be positive or negative, and for $\langle C\rangle = 1/2$, the distribution $p(c)$ has a zero mean and is obviously symmetric.

We study the following kinetic equation for $p(c)$, formally identical to (3.9) in § 3:

$$\partial_t p = n\left(-p + p^{\otimes 1+1/n}\right), \tag{B 1}$$

where n is a positive number, and the time t is dimensionless. The concentration c being a positive or negative real number, we define the Fourier transform $\tilde{p}(k)$ of $p(c)$ as

$$\tilde{p}(k) = \int \mathrm{e}^{\mathrm{i}kc}\, p(c)\,\mathrm{d}c. \tag{B 2}$$

The Fourier transform of (B 1) thus becomes

$$\partial_t \tilde{p} = n\left(-\tilde{p} + \tilde{p}^{1+1/n}\right). \tag{B 3}$$

It is useful to introduce an auxiliary distribution $q(c)$ such that

$$p(c) = q(c)^{\otimes n}, \quad \text{that is} \qquad \tilde{p} = \tilde{q}^{\,n}, \tag{B 4}$$

and check that its evolution equation is

$$\partial_t \tilde{q} = -\tilde{q} + \tilde{q}^2. \tag{B 5}$$

The moments of $p(c)$ are generated by $\langle c^m \rangle = (i)^m \partial^m \tilde{p}/\partial k^m$. We have $\langle c \rangle = 0$, and we call $\sigma^2 = \langle c^2 \rangle$ the variance of $p(c)$. Now $p(c)$ has a zero mean, and so has $q(c)$. Therefore, we call σ_q^2 the variance of $q(c)$. Clearly, $\sigma^2 = n\sigma_q^2$. Following the procedure in § 3, we look for an asymptotic similarity solution for $q(c)$ by introducing a scaled distribution $f(\eta, \tau)$ such that

$$\left.\begin{aligned} q(c,t) &= \frac{1}{\sigma_q} f(\eta, \tau), \\ \eta &= \frac{c}{\sigma_q}, \\ \tau &= t. \end{aligned}\right\} \tag{B 6}$$

One checks that

$$\tilde{q}(k,t) = \tilde{f}(k', \tau) \quad \text{with} \quad k' = k\sigma_q. \tag{B 7}$$

From (B 5) and remembering that $\tilde{q}(0,t) = 1$ and $\partial \tilde{q}(0,t)/\partial k = 0$, one has

$$\partial_t \sigma_q = \frac{1}{2}\sigma_q. \tag{B 8}$$

Noting that

$$\frac{\partial \tilde{q}}{\partial t} = \frac{\partial \tilde{f}}{\partial k'}\frac{\partial k'}{\partial t} + \frac{\partial \tilde{f}}{\partial \tau}\frac{\partial \tau}{\partial t} = k'\frac{\partial \tilde{f}}{\partial k'}\left(\frac{1}{\sigma_q}\frac{\partial \sigma_q}{\partial t}\right) + \frac{\partial \tilde{f}}{\partial \tau}, \tag{B 9}$$

one obtains the evolution equation for $f(k')$, which in the asymptotic stationary limit (letting $\partial \tilde{f}/\partial \tau \to 0$) is

$$k'\partial_{k'} \tilde{f} = 2(-\tilde{f} + \tilde{f}^2) \tag{B 10}$$

whose solution, satisfying $\partial^2 \tilde{f}/\partial k'^2 = -1$ by definition, is

$$\tilde{f} = \frac{1}{1 + \dfrac{k'^2}{2}} \tag{B 11}$$

and whose inverse Fourier transform provides $q(c)$ as

$$q(c) = \frac{1}{2\sigma_q} \mathrm{e}^{-|c|/\sigma_q}. \tag{B 12}$$

Finally, the distribution $p(c)$ is obtained from the inverse Fourier transform of (B 11) raised to the power n, since $\tilde{p} = \tilde{q}^n$, that is

$$\tilde{p} = \frac{1}{\left(1 + \dfrac{(k\sigma)^2}{2n}\right)^n}, \tag{B 13}$$

which means

$$p\left(x = \frac{c}{\sigma}\right) = \frac{2^{3/4-n/2}\, n^{n/2+1/4}\, |x|^{n-1/2} K_{1/2-n}(\sqrt{2n}\,|x|)}{\sqrt{\pi}\,\Gamma(n)}, \tag{B 14}$$

where $K_{1/2-n}$ is the modified Bessel function of the third kind and the order $1/2 - n$. The shape of $p(x)$ is displayed in figure 24 for various values of n. As expected, this shape goes from singular and cusped to round and bell-like as n increases, all with

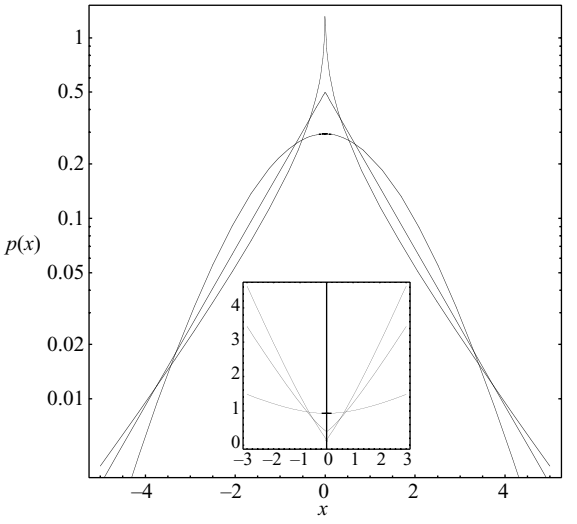

FIGURE 24. Distributions $p(x)$ given by (B 14) for various values of n: cusped shape, $n = 0.5$; tent shape, $n = 1$; bell shape, $n = 10$. Insert: corresponding conditional dissipation.

symmetric exponential wings. This one-parameter family of distributions is the strict analogue of the gamma distributions in (2.2), generalized to a situation in which the convolution construction is made for the fluctuations around the mean and not from $C = 0$ (see also Villermaux, Stroock & Stone 2008 for an application).

The concentration gradient squared conditioned to c in that case gives

$$\frac{\langle(\nabla c)^2 \,|\, x = c/\sigma\rangle}{\langle(\nabla c)^2\rangle} = -\frac{2}{p(x)}\left[\int_x^\infty \mathrm{d}x_1 \int_{x_1}^\infty \mathrm{d}x_2\, n \frac{\partial}{\partial n}\left(\frac{p(x_2, n)}{n}\right)\right] \tag{B 15}$$

and has a symmetric U shape (see § 5.2), as seen in figure 24.

REFERENCES

ALLÈGRE, C. J. & TURCOTTE, D. L. 1986 Implications of a two-component marble-cake mantle. *Nature* **323**, 123–127.

ARNOLD, V. I. & AVEZ, A. 1967 *Problèmes Ergodiques de la Mécanique Classique*. Gauthier–Villars Editeur.

BALMFORTH, N. J. & YOUNG, W. R. 2003 Diffusion-limited scalar cascades. *J. Fluid Mech.* **482**, 91–100.

BATCHELOR, G. K. 1959 Small-scale variation of convected quantities like temperature in a turbulent fluid. Part 1. General discussion and the case of small conductivity. *J. Fluid Mech.* **5**, 113–133.

BEIGIE, D., LEONARD, A. & WIGGINS, S. 1991 A global study of enhanced stretching and diffusion in cahotic tangles. *Phys. Fluids* A **3** (5), 1039–1050.

BETCHOV, R. 1956 An inequality concerning the production of vorticity in isotropic turbulence. *J. Fluid Mech.* **1**, 497–504.

BUCH, K. A., JR & DAHM, W. J. A. 1996 Experimental study of the fine-scale structure of conserved scalar mixing in turbulent shear flows. Part 1. $Sc \gg 1$. *J. Fluid Mech.* **317**, 21–71.

CELANI, A. & SEMINARA, A. 2005 Large-scale structure of passive scalar turbulence. *Phys. Rev. Lett.* **94**, 214503.

CHEN, H., CHEN, S. & KRAICHNAN, R. H. 1989 Probability distribution of a stochastically advected scalar field. *Phys. Rev. Lett.* **63**, 2657.

CHERTKOV, M., KOLOKOLOV, I. & LEBEDEV, V. 2007 Strong effect of weak diffusion on scalar turbulence at large scales. *Phys. Fluids* **19** (10), 101703.

Clay, P. H. 1940 The mechanism of emulsion formation in turbulent flow. 1. Experimental part. *Proc. R. Acad. Sci.* (*Amsterdam*) **43**, 852–865.

Corrsin, S. 1951 On the spectrum of isotropic temperature fluctuations in an isotropic turbulence. *J. Appl. Phys.* **22**, 469–473.

Curl, R. L. 1963 Dispersed phase mixing. I. Theory and effect in simple reactors. *AIChE J.* **9** (2), 175–181.

Danckwerts, P. V. 1953 Theory of mixtures and mixing. *Research* **6**, 355–361.

Dimotakis, P. E. & Catrakis, H. J. 1999 Turbulence, fractals and mixing. In *Mixing Chaos and Turbulence* (ed. H. Chaté, E. Villermaux & J. M. Chomaz), pp. 59–143. Kluwer Academic/Plenum.

Dopazo, C. 1979 Relaxation of initial probability density function in the turbulent convection of scalar fields. *Phys. Fluids* **22** (1), 20–30.

Dopazo, C. 1994 Recent developments in pdf methods. In *Turbulent Reacting Flows* (ed. P. A. Libby & F. A. Williams), chapter 7. Academic Press.

Duplat, J. & Villermaux, E. 2000 Persistency of material element deformation in isotropic flows and growth rate of lines and surfaces. *Eur. Phys. J.* B **18**, 353–361.

Eaton, J. K. & Fessler, J. R. 1994 Preferential concentration of particles by turbulence. *Intl J. Multiphase Flows* **20**, 169–209.

Eswaran, V. & Pope, S. B. 1988 Direct numerical simulation of the turbulent mixing of a passive scalar. *Phys. Fluids* **31** (3), 506–520.

Falkovich, G., Gawedzki, K. & Vergassola, M. 2001 Particles and fields in fluid turbulence. *Rev. Mod. Phys.* **73** (4), 913–975.

Fannjiang, A., Nonnenmacher, S. & Wolonski, L. 2004 Dissipation time and decay of correlations. *Nonlinearity* **17**, 1481–1508.

Feller, W. 1970 *An Introduction to Probability Theory and Its Applications*. John Wiley.

Fourier, J. 1822 *Théorie Analytique de la Chaleur*. Firmin Didot.

Fox, R. O. 1994 Improved Fokker–Planck model for the joint scalar, scalar gradient pdf. *Phys. Fluids* **6** (1), 334–348.

Fox, R. O. 2004 *Computational Models for Turbulent Reacting Flows*. Cambridge University Press.

Fox, R. O. & Raman, V. 2004 A multienvironment conditional probability density function model for turbulent reacting flows. *Phys. Fluids* **16**(12), 4551–4565.

Friedlander, S. K. & Wang, C. S. 1966 The self-preserving particle size distribution for coagulation by Brownian motion. *J. Colloid Interface Sci.* **22**, 126–132.

Frisch, U. 1995 *Turbulence*. Cambridge University Press.

Gibbs, J. W. 1981 *Elementary Principles in Statistical Mechanics*. Reprint edition. Ox Bow Press.

Girimaji, S. S. & Pope, S. B. 1990 Material–element deformation in isotropic turbulence. *J. Fluid Mech.* **220**, 427–458.

Hinze, J. O. 1955 Fundamentals of the hydrodynamic mechanism of splitting in dispersion processes. *AIChE J.* **1** (3), 289–295.

Holzer, M. & Siggia, E. D. 1994 Turbulent mixing of a passive scalar. *Phys. Fluids* **6** (5), 1820–1837.

Jayesh & Warhaft, Z. 1992 Probability distributions, conditional dissipation, and transport of passive temperature fluctuations in grid-generated turbulence. *Phys. Fluids* A **4** (10), 2292–2307.

Kimura, Y. & Kraichnan, R. H. 1993 Statistics of an advected passive scalar. *Phys. Fluids* A **5** (9), 2264–2277.

Lavertu, A. & Mydlarski, L. 2005 Scalar mixing from a concentrated source in a turbulent channel flow. *J. Fluid Mech.* **528**, 135–172.

Lei, X., Ackerson, B. J. & Tong, P. 2001 Settling statistics of hard sphere particles. *Phys. Rev. Lett.* **86** (15), 3300–3303.

Levèque, M. A. 1928 Les lois de la transmission de la chaleur par convection. *Ann. Mines* **13**, 201–239.

Marble, F. E. 1988 Mixing, diffusion and chemical reaction of liquids in a vortex field. In *Chemical Reactivity in Liquids: Fundamental Aspects* (ed. M. Moreau & P. Turq). Plenum.

Marble, F. E. & Broadwell, J. E. 1977 The coherent flame model for turbulent chemical reactions. *Project SQUID, Tech. Rep.* TRW-9-PU.

Mayer, J. E. & Mayer, M. G. 1966 *Statistical Mechanics*. John Wiley.

Meunier, P. & Villermaux, E. 2003 How vortices mix. *J. Fluid Mech.* **476**, 213–222.

Mohr, W. D., Saxton, R. L. & Jepson, C. H. 1957 Mixing in laminar-flow systems. *Ind. Engng Technol.* **49** (11), 1855–1856.

Obukhov, A. M. 1949 Structure of the temperature field in a turbulent flow. *Izv. Acad. Nauk SSSR, Geogr. i Geofiz* **13**, 58–69.

Ottino, J. M. 1989 *The Kinematics of Mixing: Stretching, Chaos, and Transport*. Cambridge University Press.

Pope, S. B. 1985 Pdf methods for turbulent reacting flows. *Prog. Energy Combust. Sci.* **11**, 119–192.

Pope, S. B. 2000 *Turbulent Flows*. Cambridge University Press.

Pumir, A. 1994 A numerical study of the mixing of a passive scalar in three dimensions in the presence of a mean gradient. *Phys. Fluids* **6** (6), 2118–2132.

Pumir, A., Shraiman, B. I. & Siggia, E. D. 1991 Exponential tails and random advection. *Phys. Rev. Lett.* **66** (23), 2984–2987.

Ranz, W. E. 1979 Application of a stretch model to mixing, diffusion and reaction in laminar and turbulent flows. *AIChE J.* **25**(1), 41–47.

Rhines, P. B. & Young, W. R. 1983 How rapidly is a passive scalar mixed within closed streamlines. *J. Fluid Mech.* **133**, 133–145.

Sawford, B. L. 2004 Conditional scalar mixing statistics in homogeneous isotropic turbulence. *New J. Phys.* **6,** 55.

Schlichting, H. 1987 *Boundary Layer Theory*. McGraw-Hill.

Schumacher, J., Sreenivasan, K. R. & Yeung, P. K. 2005 Very fine structures in scalar mixing. *J. Fluid Mech.* **531**, 113–122.

Sinai, Ya., G. & Yakhot, V. 1989 Limiting probability distributions of a passive scalar in a random velocity field. *Phys. Rev. Lett.* **63**, 1962–1964.

Sreenivasan, K. R. 1991 On local isotropy of passive scalars in turbulent shear flows. *Proc. R. Soc. Lond.* A **434**, 165–182.

Stone, H. A. 1994 Dynamics of drop deformation and breakup in viscous fluids. *Annu. Rev. Fluid Mech.* **26**, 65–102.

Venaille, A. & Sommeria, J. 2007 A dynamical equation for the distribution of a scalar advected by turbulence. *Phys. Fluids* **19** (2), 028101.

Villermaux, E. & Duplat, J. 2003 Mixing as an aggregation process. *Phys. Rev. Lett.* **91** (18), 184501.

Villermaux, E. & Duplat, J. 2006 Coarse-grained scale of turbulent mixtures. *Phys. Rev. Lett.* **97** (14), 144506.

Villermaux, E. & Innocenti, C. 1999 On the geometry of turbulent mixing. *J. Fluid Mech.* **393**, 123–145.

Villermaux, E., Innocenti, C. & Duplat, J. 1998 Histogramme des fluctuations scalaire dans le mlange turbulent transitoire. *C. R. Acad. Sci. Paris* **326** (Série), 21–26.

Villermaux, E., Innocenti, C. & Duplat, J. 2001 Short circuits in the Corrsin–Oboukhov cascade. *Phys. Fluids* **13** (1), 284–289.

Villermaux, E. & Rehab, H. 2000 Mixing in coaxial jets. *J. Fluid Mech.* **425**, 161–185.

Villermaux, E., Stroock, A. D. & Stone, H. A. 2008 Bridging kinematics and concentration content in a chaotic micromixer. *Phys. Rev.* E **77** (1, Pt 2), 015301.

Von Smoluchowski, M. 1917 Versuch einer mathematischen theorie der koagulationskinetik kolloider losungen. *Z. Phys. Chem.* **92**, 129–168.

Voth, G. A., Haller, G. & Gollub, J. P. 2002 Experimental measurements of stretching fields in fluids. *Phys. Rev. Lett.* **88** (25), 254501.

Warhaft, Z. 1984 The interference of thermal fields from line sources in grid turbulence. *J. Fluid Mech.* **144**, 363–387.

Warhaft, Z. 2000 Passive scalars in turbulent flows. *Annu. Rev. Fluid Mech.* **32**, 203–240.

Zeldovich, Y. B. 1937 The asymptotic law of heat transfer at small velocities in the finite domain problem. *Zhurnal Eksp. i Teor. Fiz.* **7** (12), 1466–1468.